State of the art on microbubble cavitation monitoring and feedback control for blood-brain-barrier opening using focused ultrasound

Paul Mondou, Sébastien Mériaux, Florent Nageotte, Jonathan Vappou, Anthony Novell, Benoit Larrat

Physics in Medicine & Biology

IPEM Institute of Physics and Engineering in Medicine

ACCEPTED MANUSCRIPT

State of the art on microbubble cavitation monitoring and feedback control for blood-brain-barrier opening using focused ultrasound

To cite this article before publication: Paul Mondou *et al* 2023 *Phys. Med. Biol.* in press https://doi.org/10.1088/1361-6560/ace23e

State of the art on microbubble cavitation monitoring and feedback control for blood-brain-barrier opening using focused ultrasound

Paul Mondou[1,2], Sébastien Mériaux[2], Florent Nageotte[1], Jonathan Vappou[1], Anthony Novell[2,3], Benoit Larrat[2]*

[1] *Université de Strasbourg, CNRS, ICube, UMR7357, Strasbourg, France*

[2]*Université Paris-Saclay, CEA, CNRS, Joliot, DRF, BAOBAB, Neurospin, 91191, Gif-sur-Yvette, France*

[3]*Université Paris-Saclay, CEA, CNRS, Inserm, BioMaps, SHFJ, 91401, Orsay, France*

**Author to whom any correspondence should be addressed.*

E-mail : benoit.larrat@cea.fr

Focused ultrasound is a non-invasive and highly promising method for targeted and reversible blood-brain barrier permeabilization. Numerous preclinical studies aim to optimize the localized delivery of drugs using this method in rodents and non-human primates. Several clinical trials have been initiated to treat various brain diseases in humans using simultaneous BBB permeabilization and drug injection. This review presents the state of the art of *in vitro* and *in vivo* cavitation control algorithms for BBB permeabilization using microbubbles and focused ultrasound. Firstly, we describ the different cavitation states, their physical significance in terms of microbubble behavior and their translation into the spectral composition of the backscattered signal. Next, we report the different indexes calculated and used during the ultrasonic monitoring of cavitation. Finally, the different *in vitro* and *in vivo* cavitation control strategies described in the literature are presented and compared.

1 Introduction

Focused ultrasound (FUS) is highly promising, non-invasive approach that offers the possibility to destroy pathological tissues, either thermally or mechanically, or to enhance drug delivery(Izadifar *et al* 2020, Quadri *et al* 2018, Pandit *et al* 2020). Ultrasound focusing allows increasing the acoustic pressure in the focal zone. Biological effects resulting from tissue/ultrasound interactions depend on the sonication parameters (*e.g.*, waveform, amplitude, frequency, duration of emission and duty cycle) and tissue properties (*e.g.*, density, celerity, absorption). For instance, tissue destruction can be achieved through thermal effects by long sonications (typically tens of seconds or minutes) at moderate acoustic pressure (typically a few MPa), or through mechanical effects, such as histotripsy, which uses repeated microsecond-range sonications at very high acoustic pressure (typically a few tens of MPa)(Bader *et al* 2019, Geoghegan *et al* 2022).

The appearance and subsequent oscillations or collapses of gas microbubbles (MBs) is an acoustic phenomenon called cavitation. When properly controlled, cavitation can be taken advantage of in focused ultrasound therapies by adjusting the ultrasound energy required to induce bioeffects. During thermal ablation the presence of MBs in the target region strongly increases the local absorption of the ultrasound energy and thus boosts thermal deposition while preserving remote

tissue(Tung *et al* 2006, Lo *et al* 2006). In high intensity histotripsy, large negative pressures create a cloud of MBs of dissolved gas that destroys the tissue through implosion (Hoogenboom *et al* 2015).

Though cavitation can occur without injected MBs, exogenous ultrasound contrast agents may also act as cavitation nuclei. First use of injected MBs in the context of therapeutic ultrasound was mentioned shortly before 2000 (Miller and Thomas 1995, Poliachik *et al* 1999, Tran *et al* 2003). Injected MBs can create similar cavitation effects as endogenous MBs under ultrasound exposure, without the need for risky peak negative pressure values that are required for endogenous MBs to appear(Tran *et al* 2003). Moreover, the properties, amount and location of the MBs are also controlled more accuretely.

Beyond tissue destruction, the combined use of injected MBs and low-power pulsed ultrasound is also known to induce reversible effects on cell membranes and vascular walls. Indeed, compression/dilation of MBs induce fluid micro-streaming as well as direct mechanical forces on surrounding cell membranes, resulting in temporary permeabilization, an effect known as sonoporation (van Wamel *et al* 2006, Yang *et al* 2020). A similar phenomenon occurs in the cerebral capillaries, leading to a reversible permeabilization of the blood-brain barrier (BBB). During FUS-induced BBB opening, MBs oscillate and induce fluid streaming within a diameter's range away from their surface. This leads to the loosening of tight junctions in between endothelial cells, allowing large molecules to enter the brain in the sonicated area(Cammalleri *et al* 2020, Hynynen *et al* 2001, Sheikov *et al* 2004). In addition, microbubble-assisted focused-US can also alter the gene expression of essential BBB efflux transport proteins, such as downregulation of the P-glycoprotein, which enhances medication localization in the parenchyma(Jangjou *et al* 2021, Aryal *et al* 2017, Conti *et al* 2022). However, it is difficult to understand the precise mechanism of interactions between MBs and tissues leading to BBB disruption(Barzegar-Fallah *et al* 2022).

Regarding this later application, cavitation must be carefully controlled to ensure safety and efficacy(Dauba *et al* 2020a). Excessive acoustic pressure can cause MBs to implode resulting in pressure forces that will cause significant vascular or tissue damages such as hemorrhages and edemas. On the contrary, if the acoustic pressure is insufficient, the BBB remains intact. The pressure range that allows BBB opening without damage is narrow, since it typically spans over several tens of kPa(Ilovitsh *et al* 2018). For instance, (Tung *et al* 2010) reported a 300 to 450 kPa range, (Xu *et al* 2019b) reported a range of 250 to 500 kPa, and (Baseri *et al* 2010) reported a range of 300 to 460 kPa. It should be noted that the occurrence of stable cavitation during BBB opening depends on various factors, including frequency, pressure, pulse length, duration, bubble type, bubble size, bubble dose, and animal model. The non-linearity of cavitation with respect to pressure as well as the heterogeneities of the propagation media (skull, tissue) make the control of BBB opening rather challenging. The transmission of ultrasound through the skull is affected not only by the absorption of the bone and the tissues, but also by the reflections and refractions at each interface between media with different acoustic impedances (e. g. tissue, bone, bone marrow). As a result, the ultrasound beam is deflected and its intensity is reduced in a unique way for each individual and target in the brain. This effect is more pronounced in larger animal species with thicker skulls. Numerical simulations including patient-specific head modeling are particularly appropriate for mitigating these effects (Angla *et al* 2023). However, this approach is computationally demanding and may suffer from uncertainties regarding the physical properties of tissues *in vivo* and imprecision in terms of 3D pressure profile quantification. Alternatively, monitoring cavitation activity in real time can ensure that the appropriate dose of ultrasound is delivered to consistently disrupt the BBB across the skull without causing vascular damage.

Magnetic resonance imaging (MRI) can be used for several purposes, such as positioning (Liu *et al* 2015), measuring thermal effects (Rademaker *et al* 2003, Rieke and Butts Pauly 2008), and monitoring treatment effectiveness. However, it is not currently used to track cavitation and MBs state. Instead, cavitation can be monitored by analyzing the ultrasound signal backscattered by the MBs during sonication. Multiple indexes are computed for the real-time analysis of backscattered spectra, which are then used as inputs to various cavitation control algorithms to modulate the acoustic intensity of the therapeutic wave. This review aims to provide an overview of the various methods proposed in the literature for monitoring cavitation and their different and sometimes controversial uses.

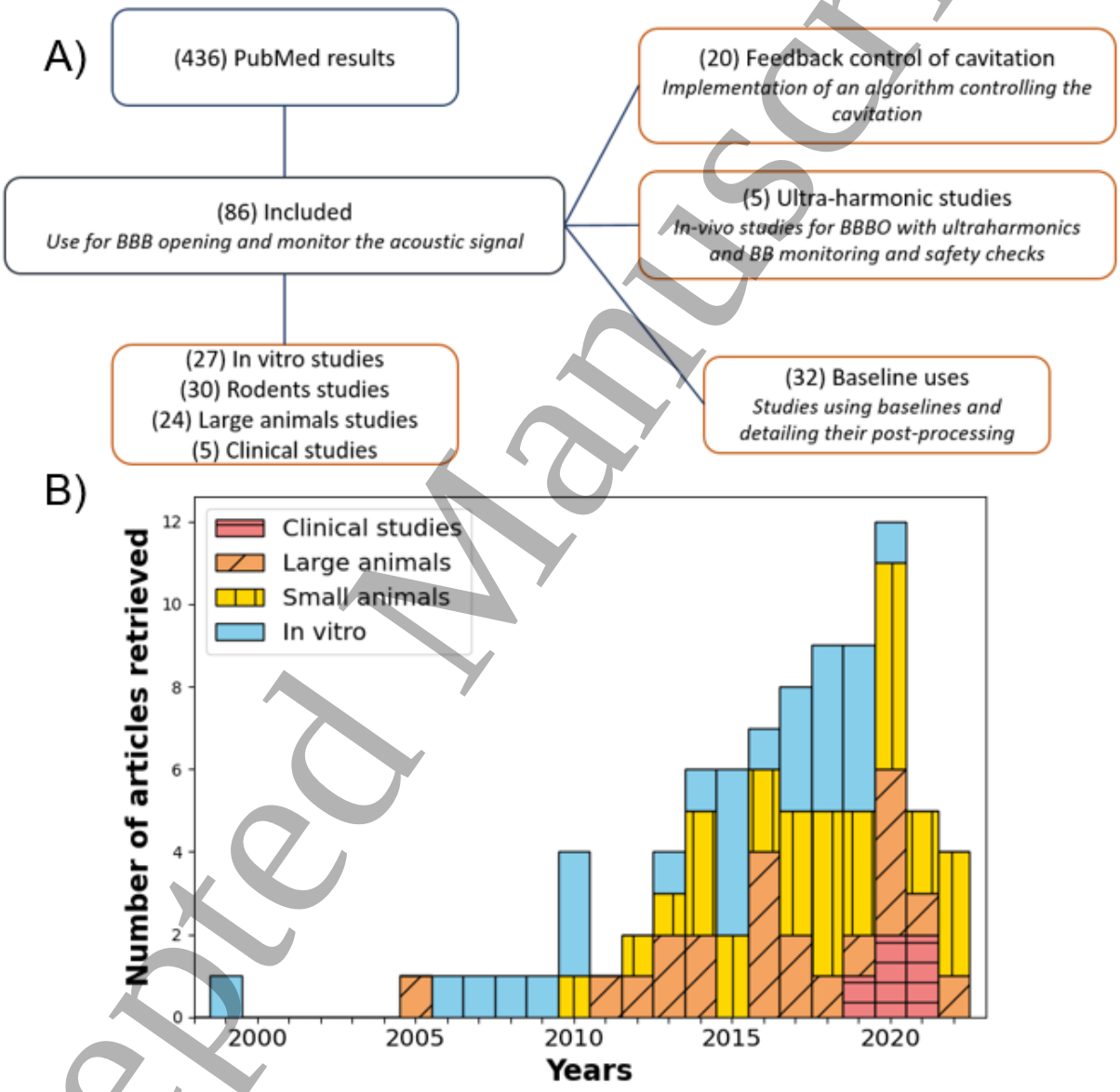

Figure 1: *A) Flowchart illustrating the inclusion of articles in the review based on PubMed results. On the right side, the diagram showcases the diverse ways in which the included articles are used within the review. B) Graph showing the number of articles retrieved and included in the review by year showing the growing interest of this topic in medical research.*

A search was conducted on PubMed using the following keywords: (("blood-brain barrier" OR BBB) AND "cavitation") OR ("stable cavitation" and (monitor OR control)) OR ((microbubbles AND ultrasound AND monitoring AND cavitation) OR ((ultrasound) AND (microbubbles) AND ((cavitation AND monitoring AND focused) OR (cavitation AND focused AND therapy) OR (monitoring AND focused AND therapy))))). A total of 436 articles were found and analyzed (Figure 1). After a review of their titles and abstracts, nearly 200 articles were discarded because they did not address BBB opening or only mentioned it without monitoring it. Some articles that used BBB opening without monitoring the backscattered acoustic signal were also removed as they did not contribute to this review. The remaining articles underwent a thorough review to assess their relevance, excluding those lacking sufficient details on their protocol, calculation methods, or those duplicating protocols previously described elsewhere. Ultimately, a total of 86 articles focusing on cavitation monitoring and control, as well as the nonlinear emissions of sonicated microbubbles, were selected from this database.

2 Cavitation in FUS induced BBB disruption

2.1 Influence of the skull on the ultrasound propagation

In the field of focused ultrasound (FUS), one of the major challenges is to deliver therapeutic waves to the target while minimizing damage to the surrounding tissues. This is particularly difficult in the case of brain therapy, as ultrasound waves must pass through the skull, which is a dense and heterogeneous structure that affects wave propagation in a unique way for each individual. In this context, the control of cavitation is critical to ensure safety and efficacy of the treatment.

The skull bone is composed of a spongy bone, the diploe, and two external and internal tables, which are dense and compact cortical bones. The diploe has a highly heterogeneous anisotropic porous structure. The sound velocities in the bone and the bone marrow are strongly dissociated and each bone-bone marrow interface creates refractions(Pinton *et al* 2012). These factors, combined with the non-linear behavior of cavitation with respect to pressure, make the control of BBB opening a challenging task. The thicker the skulls of the animals, the more complex the ultrasound propagation through them will be(Asahara 2013, Porto *et al* 2013), and even within the same species, transmission can vary depending on the weight, sex, or size of the individual(O'Reilly *et al* 2011). If the skulls of rats and mice do not cause major differences in propagation between individuals, this is not the case for human skulls (see Table 1). Several studies have shown that the transmission factor through the human skull improves as the emission frequency decreases (Liu *et al* 2014, Pichardo *et al* 2010, White *et al* 2006). This is the reason why the frequency of emission must be reduced as the thickness of the skull increases.

In summary, the complex and heterogeneous structure of the skull poses a major challenge for the delivery of therapeutic ultrasound waves to the brain. The control of cavitation in real-time is critical to ensure that the correct dose of ultrasound is delivered to consistently disrupt the BBB across the skull without causing vascular damage. Therefore, dedicated piezoelectric sensors, called passive cavitation detectors (PCD), are generally used to record the backscattered cavitation signal from the sonicated MBs. PCDs need to be sensitive over a large frequency bandwidth and be placed where the skull attenuation is minimum (typically close to the temporal bone). In the next sections, we will present an overview of the different approaches proposed in the literature to monitor and control cavitation during FUS brain therapy.

Skull of :	Mice	Rats	NHP	Humans
Transmission factor	85% at 1.5MHz (Felix *et al* 2021)	60% at 1.5MHz (Gerstenmayer *et al* 2018)	40% at 600kHz (Deffieux and Konofagou 2010)	24% at 500kHz (Deffieux and Konofagou 2010)

Table 1: *Ultrasound transmission factor for the parietal bone of mice, rats, Non-Human-Primate (NHP) and humans at different frequencies (ex vivo experiments). As a general trend, reducing the frequency of ultrasound emission improves transmission through thicker skulls. However, for the thinnest skulls (such as rodents), higher frequencies are used to avoid creating larger focal spots that may not be adapted for their smaller brains.*

2.2 Cavitation regimes

Studies have shown that the increasing *in situ* pressure is correlated with an increase in the permeabilization of the BBB(McDannold *et al* 2008, Chu *et al* 2016). This permeabilization only appears from a certain pressure threshold depending on the animal species, weight and age, the choice of the ultrasound frequency, the characteristics of the MBs, the concentration of MBs, and the vascularization in the focal region. The permeability enhancement is accompanied by an increase in the size of the molecules that can enter into the brain (Chen and Konofagou 2014). Above a 2nd pressure threshold, the MBs will start to collapse, which results in vascular damage. Two cavitation regimes can be differentiated: the stable cavitation and the inertial cavitation. Under stable cavitation, the MBs oscillations (push-pull mechanism) along the endothelial cells induce tight junction disruption and safe BBB permeabilization(McDannold *et al* 2006). On the contrary, inertial cavitation is commonly associated with tissue damage. Collapse of MBs causes shock waves (Leighton 1994) and micro-jets (Blake and Gibson 1987). These forces are responsible for damage to vessels and organs.

The backscattered signal from MBs can be detected and exploited in cavitation control algorithms as a feedback source. This signal can be recorded by piezoelectric receivers (Everbach *et al* 1997). The regime of MBs oscillations can be deduced from the spectral decomposition of the backscattered signal (Coussios and Roy 2008). Multiple frequency responses can be extracted from the backscattered signal: the fundamental f_0, its harmonics ($n * f_0; n \in \mathbb{N}^*$), the subharmonic (SH) $f_0/2$ and its multiples called ultra-harmonics (UH) ($(n + 1/2) * f_0; n \in \mathbb{N}^*$) and the broadband noise. Broadband noise can be defined by the enhancement of the noise level in the frequencies range.

2.3 Origin of the various cavitation signature

MBs consist of a gaseous core, mostly made of an inert gas, surrounded by a shell protecting the gas from diffusion. Typical MBs are between 0.5 and 10µm in diameter, and circulate for a few minutes in the bloodstream after an intravenous injection. When the MBs undergo small amplitude oscillations, the backscattered signal is solely composed of fundamental, harmonic, subharmonic and ultra-harmonics components of the transmitted signal. Under ultrasound exposure, the shell can destabilize, buckle, shed its lipids or even diffuse gas, which increases the non-linearity of the MBs response(Shi and Forsberg 2000, Leighton 1994). As the acoustic pressure increases, the MB oscillations intensify, together with the nonlinear emissions. These modifications of the envelope properties can be observed through the increase of the SH and UH components (Figure 2). Furthermore, SH emissions can arise from various mechanisms, including the route to chaos phenomenon (Parlitz *et al* 1990, Lauterborn and Kurz 2010, Lauterborn and Cramer 1981), and the excitation of a bubble with an equilibrium radius twice the resonance radius. As the pressure continues

to increase, MBs will finally collapse, emitting a broadband noise (Chen *et al* 2003, Everbach *et al* 1997, Yasui 2023). The observations suggest that the collapse of MBs generates periodic shock-emissions within acoustically driven cavitation clouds, which also emits the SH component(Johnston *et al* 2014). Indeed, when a MB collapses, the pressure forces generated lead the nearby MBs to collapse as well(Apfel 1982, Delalande *et al* 2013, Leighton 1994). This sequence of events appears very quickly and will emit an impulse signal which will be characterized in the frequency domain by a very large-band emission. The interactions between MB and solid walls influence heat and mass transfer, bubble dynamics, and fluid flow patterns, leading to alterations in the overall behavior of MBs in the free field(Klaseboer and Khoo 2004).

It should be noted that while these phenomena have been observed and studied, there may be other bubble dynamics yet to be fully understood due to the complex physics of bubble behavior(Lauterborn and Kurz 2010). One can mention that the backscattered signal corresponds to the averaged response of a cloud of MBs oscillating in different regimes.

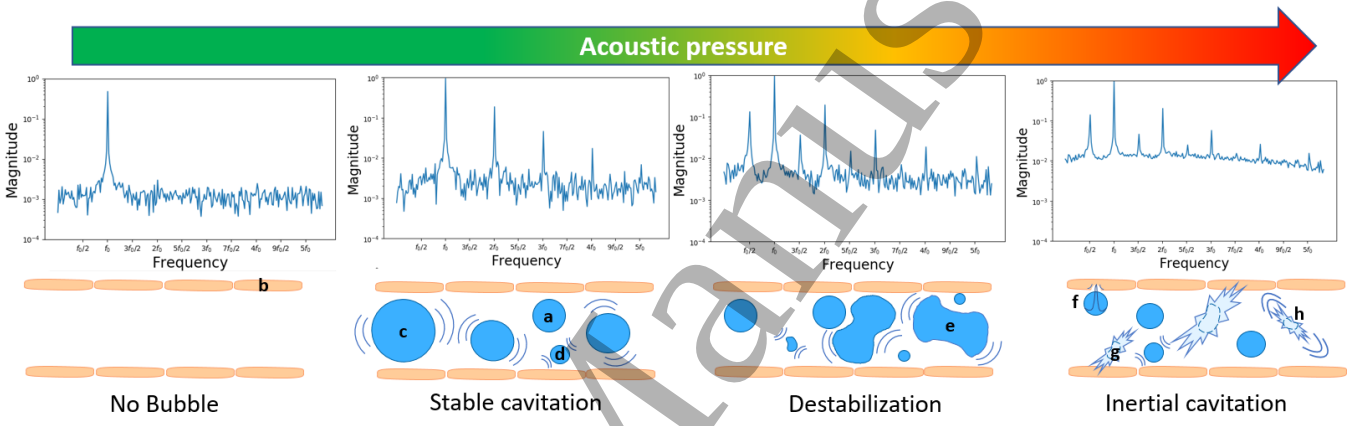

Figure 2: *Cavitation state of MBs and typical associated spectra. The microbubbles (**a**) flow between the brain endothelial cells (**b**). The stable cavitation induces a push- (**c**) pull (**d**) mechanism. Upon destabilization, the MBs envelope is deformed (**e**); and inertial cavitation induces micro jetting (**f**), fragmentation (**g**) and shock waves (**h**) that can damage brain capillaries.*

2.4 PCD transducer technologies

Different types of transducers are currently used for PCD that can be sorted according to the number of reception elements, the ratio between the reception and transmission frequency, the transducer technologies used (table 2), the shape, and the positioning of the transducers during the sonication.

Material	Sensitivity	Bandwidth
Piezocomposite (Chapelon *et al* 2000)	High	Low
PZT (Zhang *et al* 2006)	Medium	Medium
PVDF(Foster *et al* 2000)	Low	Very high
CMUT(Dauba *et al* 2020b)	Medium	High

Table 2: *Bandwidth and sensitivity characteristics of the different transducer technologies used for the monitoring of cavitation activity.*

Materials commonly used are ferroelectrics (lead zirconate titanate commonly abbreviated as PZT) and polymers (polyvinylidene fluoride abbreviated as PVDF). Although they are more complex to produce, piezocomposites show a higher electromechanical coupling coefficient than basic PZT ceramics resulting in an improved signal to noise ratio and a better signal detection. Recently, Capacitive Micromachined Ultrasonic Transducer (CMUT), have shown an interesting potential for PCD *ex vivo* offering a tradeoff between sensitivity and bandwidth. The transducers (emitter and receiver) are positioned on the top of the animal's skull for rodents. Rodents are either placed in a supine or prone position depending on the configuration of the ultrasound device. For macaques, the transducers are placed normal to the skull and positioned to allow for optimal targeting of the selected brain sections. The most commonly observed brain regions are the following: putamen, thalamus, striatum, hippocampus. These are paired brain regions that allow comparison of the signal difference between the 2 hemispheres of the brain.

Number of elements of the PCD	**1**	**2**	**10**	**28**	**64**	**Up to 128**	**Up to 256**
Number of studies	38	1	1	1	1	6	3
Studies	(Chen and Konofagou 2014, Bing *et al* 2018, Fan *et al* 2014, Kamimura *et al* 2019, Lynch *et al* 2021, Marquet *et al* 2014, Wu *et al* 2014, Sun *et al* 2015, Wu *et al* 2016, Sun *et al* 2017, Sierra *et al* 2017, Çavuşoğlu *et al* 2019, Constans *et al* 2020, Pouliopoulos *et al* 2020b, Pascal *et al* 2020, Yang *et al* 2019, Wu *et al* 2017, Fan *et al* 2015, McMahon *et al* 2020, Lin *et al* 2017, O'Reilly and Hynynen 2010, Cheng *et al* 2019, Novell *et al* 2020, Tsai *et al* 2016, J i *et al* 2021, Xu *et al* 2019a, Tung *et al* 2011, Desjouy *et al* 2015, 2013, Boulos *et al* 2018, Xu *et al* 2019b, Zhang *et al* 2017, Chu *et al* 2016)	(Huang *et al* 2017)	(McDannold *et al* 2006)	(Lin *et al* 2020)	(Pouliopoulos *et al* 2018)	(Kamimura *et al* 2020, O'Reilly *et al* 2014, Chitnis *et al* 2019, Arvanitis *et al* 2013, Burgess *et al* 2018, Pouliopoulos *et al* 2016)	(Jones *et al* 2020, 2018, Patel *et al* 2018)

Table 3: *List of the number of transducer elements for cavitation monitoring*

The transducers used for cavitation control or monitoring are mostly single-elements (Table 3). Single-element transducers allow simplified signal processing. Some studies use multi-element transducers with up to 256 elements. The multiplicity of elements allows performing passive acoustic mapping (PAM) and get information on localization of cavitation activity. The PCD transducer can be placed inside the transmitter for a coincidence of the propagation axes (21 studies) or outside around the transmitter (23 studies). Elements can be also placed to form a half sphere enclosing the skull of the animal(Huang *et al* 2017, Jones *et al* 2018, 2020, Arvanitis *et al* 2013).

Figure 3 shows the ratios between the receiver central frequency and the transmitter frequency during cavitation control. This figure describes some technological choices made by the research groups. Many studies have a ratio close to 1 with a small bandwidth. It concerns mainly the research groups conducting research on animals and who expect to observe the SH that better cross the skull. Studies where the ratios are between 2 and 5 generally monitor the first 2 or 3 harmonics or UH. Studies with ratios between 6 and 10 are usually using a number of harmonics or UH higher than 8 or 10. Interestingly, the nonlinear response at higher harmonics can be recorded even for large animal experiments (Figure 3). Finally, several studies use broadband or flatband hydrophones that have very high central frequencies as a result of their very large bandwidth. It should be noted, though, that some groups do not use perfectly matched transducers for their experiments and may, for example, be constrained to use the same PCD transducers with different ultrasound emitters(Fan *et al* 2014, Chu *et al* 2016).

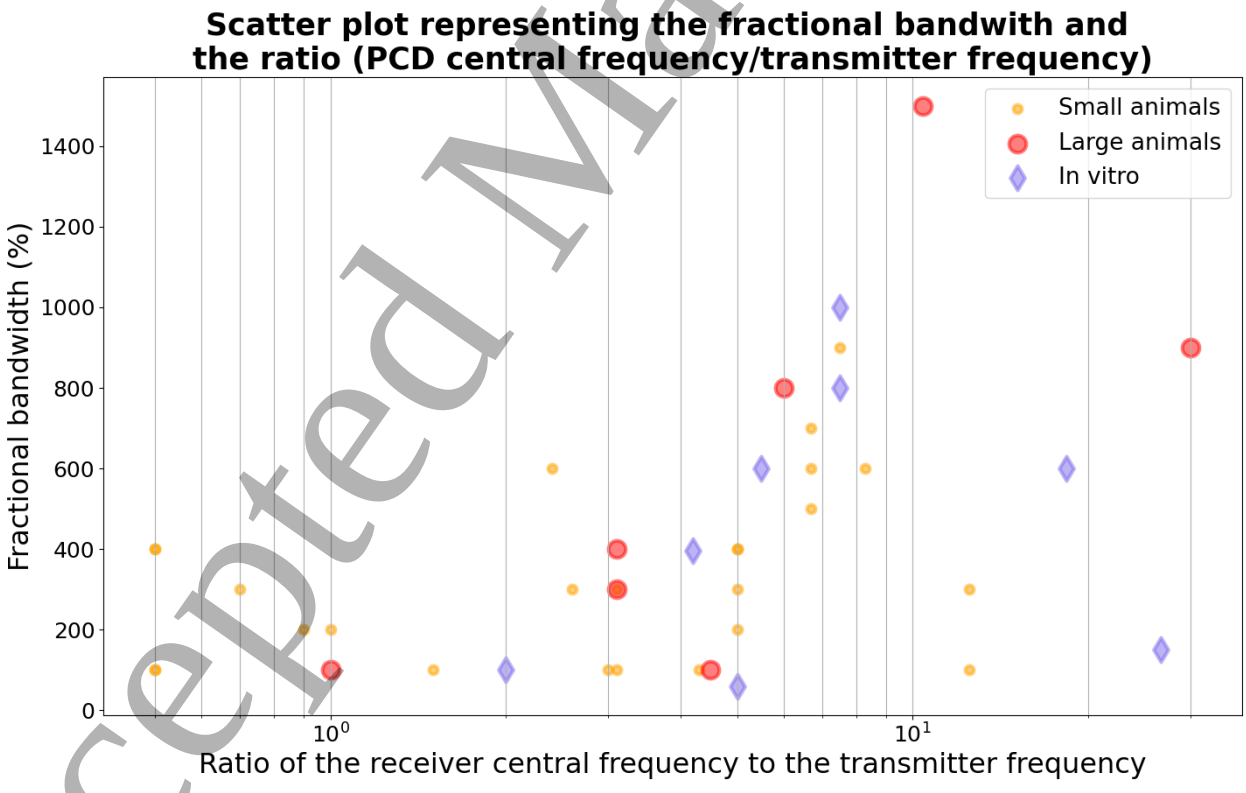

Figure 3: *Scatter plot representing on the x-axis, the ratio of the PCD central frequency to the emitted frequency. The y-axis represents the measured spectral bandwidth divided by the emitted frequency. The data can be found in S1 Table.*

2.5 Cavitation indexes

Conventionally, the most commonly reported index used for characterization of inertial cavitation is the broadband noise. Among the articles reviewed for this research, 51 report the detection of the inertial cavitation from the backscattered signal. 45 of these papers use broadband alone to characterize inertial cavitation, 4 studies use SH alone while 2 studies use a combination of broadband and SH. The characterization of stable cavitation is less consensual. For a total of 47 studies monitoring stable cavitation, 11 studies characterize stable cavitation with harmonic components only. 20 studies combine harmonics and UH, and 16 studies use only UH (Figure 4). Different indexes of stable cavitation are monitored and compared in several studies. Here, the chronology is important, as the first studies that set up cavitation monitoring used mostly harmonics, whereas the use of ultra-harmonics was reported more recently.

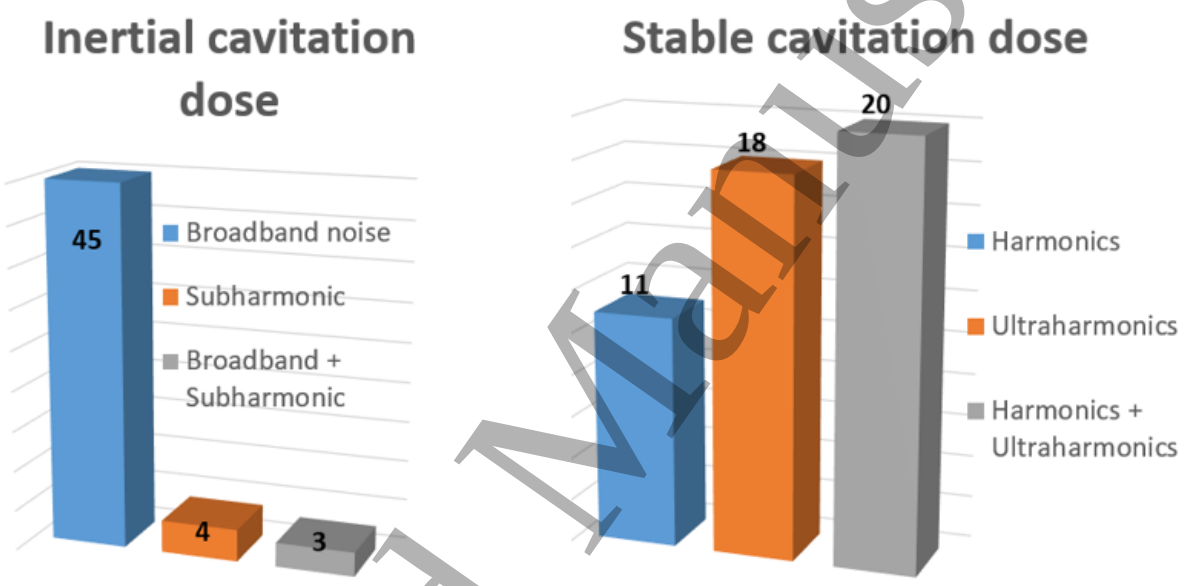

Figure 4: *Different types of frequency bands used to calculate indexes representing stable and inertial cavitation in the literature. The data can be found in S2 and S3 Tables.*

It is important to note that some studies monitor the SH component to represent inertial cavitation. From a physical point of view, the SH is generated during MB concentric deformations and the UH components appear as harmonics of this sub-multiple of f_0 (Biagi *et al* 2007). In the remainder of this review the SH will be considered as part of the UH. Some studies have focused on devices designed to be sensitive to the SH component mainly for reasons of lower skull attenuation at $f_0/2$.

Studies using PCD for cavitation monitoring use various indexes calculated from certain frequency bands surrounding harmonics and HU frequencies. The calculated value is obtained by integrating the spectrum over the frequency band or by detecting a maximum value in that band. The width of these frequency bands characterizes the sensitivity and specificity of the associated indexes. And the inertial cavitation is calculated by integrating the signal over a spectral window between the harmonics and ultra-harmonics (Figure 5).

Among the studies that monitor harmonics, $3f_0$ and $4f_0$ are the components that are the most frequently monitored (see figure 6), followed by $5f_0$ and $2f_0$. Higher harmonics are less used mainly due to the bandwidth restriction of the PCD and/or skull attenuation. Regarding the UH, the most

frequently used components are $f_0/2$ and $5f_0/2$, followed by $7f_0/2$ and $3f_0/2$. Higher UH components are less used for the same reasons (see figure 6). The UH and harmonic components are mainly centered on $3f_0$ or $4f_0$ because the frequency of the receiver transducer is mostly between 1 and 5 times the frequency of the transmitter (see Figure 6). The $2f_0$ harmonic is commonly avoided without precision from the authors, as well as the UH $3f_0/2$.

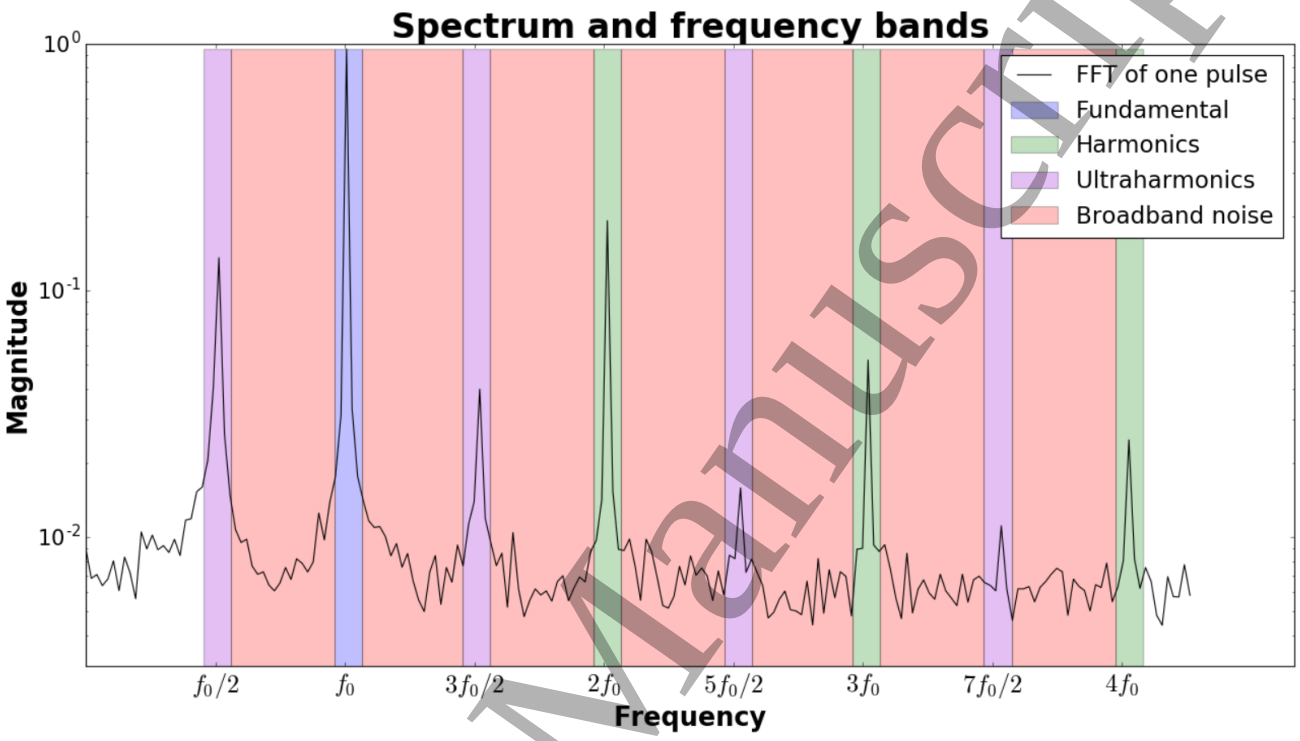

Figure 5: *Representation of the frequency bands used to calculate the indexes on a frequency spectrum of the backscattered signal obtained with a Fast Fourier Transform (FFT)*

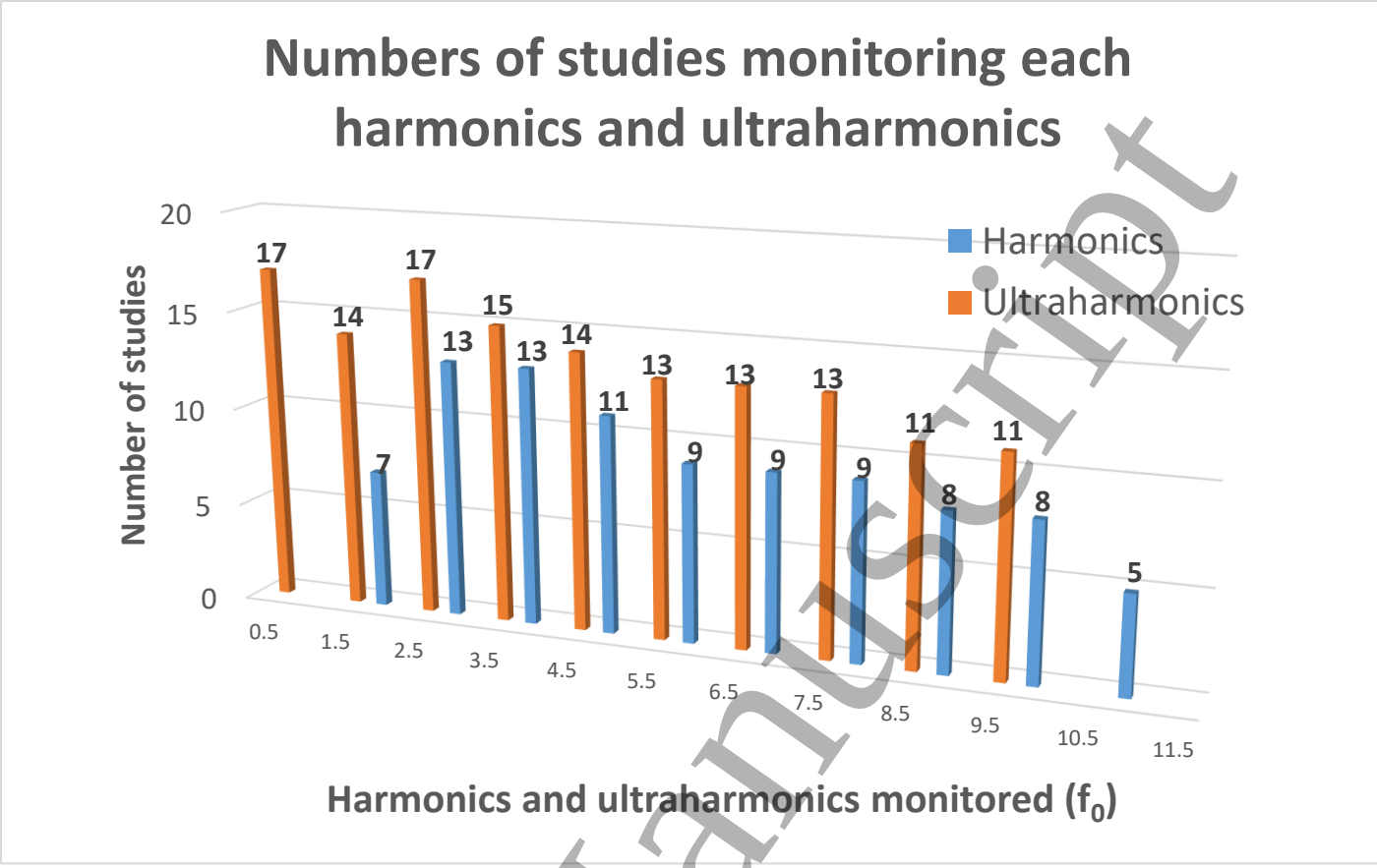

Figure 6: *Numbers of studies monitoring each different harmonics and ultraharmonic. The data can be found in S4-5 Tables.*

2.6 Baselines or reference spectra

In order to allow for more accurate cavitation monitoring, baseline spectra are acquired using different procedures. Baselines corresponding to the backscattered signal by the tissue only (*i.e.,* prior the administration of MBs) can be recorded. Among all the studies reviewed, most of them (63%) use such an acquisition to get this reference signal. This reference is then compared to the signal monitored over the treatment to extract the acoustic signature related to MBs only. Different acquisition methods can be adopted. The vast majority of studies measure the baseline signal by applying a similar acoustic pressure to the one used for treatment (addition of MBs). In some studies (Table S6), the baseline amplitude is lower than the treatment pulse amplitude. For studies allowing the modulation of the pressure amplitude over the treatment, a large range of amplitude is scanned to infer a baseline associated with each amplitude value.

The baseline can be directly used to define thresholds used in cavitation control algorithms (17%). For example, Chen and Konofagou *et al.* (Chen and Konofagou 2014) obtained the average noise level and its standard deviation from the baseline to serve as the background cavitation activity. Another option consists in using the baseline to normalize the non-logarithmic data by subtracting (E1), dividing (E2), or both (E3), the value of the monitoring indexes calculated on the spectrum with MBs by the reference value (Figure 7). It is also to be noted that some studies process (*i.e.,* divide or subtract) together baseline and MB spectra before the calculation of the indexes on the final spectrum.

While both approaches are not equivalent, most articles do not specify whether the comparison is done on the spectra or the indexes

$$Index_{substracted} = Index_{monitored} - Index_{baseline} \quad \text{(E1)}$$

$$Index_{divided} = \frac{Index_{monitored}}{Index_{baseline}} \quad \text{(E2)}$$

$$Index_{combined} = \frac{Index_{monitored} - Index_{baseline}}{Index_{baseline}} \quad \text{(E3)}$$

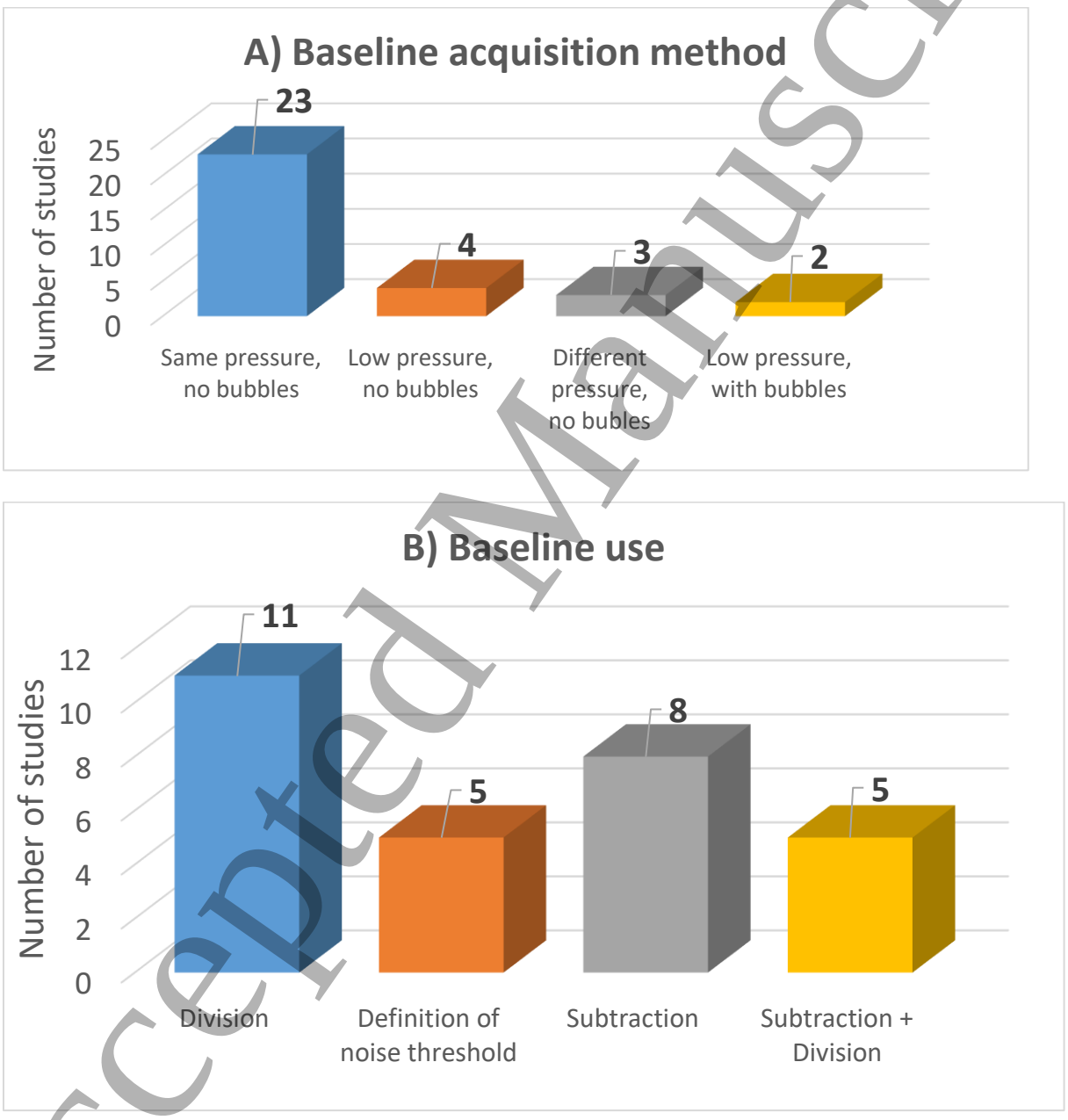

Figure 7: *Graphs representing the different processes used for obtaining the baseline (A) and their use (B). The data can be found in S6-7 Tables.*

In addition to exhibiting non-linearities coming from MBs, these various baseline procedures enable the comparison between signals obtained from experiments on different subjects or repetitive sessions on a unique subject. An effective means of comparison is a relative increase to a reference signal. The reference signal is chosen to ensure that the relative increase corresponds mostly to the state of the MBs. The variations of the propagation medium (reflection and absorption) will be observed in the baseline and will therefore be partially considered after normalization with the baseline data. In the particular context of real-time cavitation control, the baseline makes the setpoint as robust as possible to inter-subject variations.

2.7 Ultra-harmonic and sub-harmonic components and safety assessment

UH components are a point of divergence in the literature. In some studies, the occurrence of UH is considered synonymous with stable cavitation , and therefore, the detection of UH components is promoted to achieve effective BBB opening(Bing *et al* 2018). However, it is possible to effectively disrupt the BBB even without UH (or at least without detectable UH) as shown by Wu *et al*(Wu *et al* 2014). In other studies, the occurrence of UH components is considered to be indicative of possible inertial cavitation and tissue damage (O'Reilly and Hynynen, 2012). Noticeably, there is no such controversy for the interpretation of other spectral contents (harmonics and broadband noise).

It should be noted that while the appearance of UH components has been well described theoretically (Lauterborn and Kurz 2010) and in *in vitro* studies(Johnston *et al* 2014, Postema *et al* 2004), *in vivo* experiments present particular challenges. Microbubble states can vary significantly, with polydisperse sizes and capillaries of different sizes, orientations, and positions. This complexity makes simulation and modeling extremely challenging. Therefore, in this sub-section, experimental results *in vivo* are reported to provide an overview of the phenomenon.

A bibliographic analysis was conducted to identify all articles performing BBB openings and monitoring UH/SH and broadband noise. Articles were only included if the broadband noise was not detectable or if the increase from baseline was limited to 2dB. Traces of tissue damage is assessed either by MRI or histology in order to determine whether tissue damage has been observed with only UH components detected. MRI allows the observation of edemas (T_2-weighted hyperintense) and hemorrhages (T_2*-weighted hypointense). No studies used UHs in the previously defined framework before 2014. From 2014 on, only 5 peer-reviewed articles (Bing *et al* 2018, Fan *et al* 2014, Jones *et al* 2018, Kamimura *et al* 2019, Wu *et al* 2018b) meet the previously defined requirements. A total of 7 cases can be identified due to the consideration of multiple cavitation thresholds in certain studies. All of these protocols result in successful BBB opening. For each study, Table 4 compares the UH/SH cavitation thresholds (*i.e.*, the increase of the UH components compared to baseline) and the presence of damage such as hemorrhage or edema using MRI or the presence of extravasated red blood cells (ERBC) using histology. This increase often corresponds to the emergence of UH from the background noise because UH are almost never present in the baselines. Direct comparison between those studies remains difficult since cavitation detection is intrinsically associated with the sensitivity of the PCD sensor.

Reference	UH increase from baseline	Edema	Hemorrhage	ERBC	Number of animals
Fan 2014 *#1* (Fan *et al* 2014)	100%		No	Few	12 rats
Fan 2014 *#2*	200%		No	Yes	4 rats
Jones 2018(Jones *et al* 2018)	700%	Few	No	No	5 rabbits
Kamimura 2019 *#1*(Kamimura *et al* 2019)	60%	No	No		2 macaques
Kamimura 2019 *#2*	180%	No	No		1 macaque
Bing 2018(Bing *et al* 2018)	900%			No	26 rats
Wu 2018(Wu *et al* 2018b)	45%			No	3 rats

Table 4: *Results of the BBB opening studies that monitor the ultra-harmonic components while keeping the broadband noise low. Radiological and histological findings, Type and number of animals used.*

The finding of vascular damage in studies in which UH components were detected is very unusual if the enhancement of the UH from baseline remains low (*i.e.*, inferior to 200%). However, many studies were excluded because of the broadband noise level, so it is likely that the significant UH enhancement in the Bing *et al* study comes from a better sensitivity of their equipment compared with that used by Fan *et al*. No study reported high UH level and low broadband noise simultaneously. Thus, UH can be considered as precursors of broadband noise and inertial cavitation in BBBO experiments, as predicted by theoretical approaches. Indeed, the emission of UH components does not necessarily mean that vascular damage will occur, but rather that inertial cavitation is very likely to occur if the ultrasound pressure is held constant or increased further.

3 Cavitation feedback control in the literature

We have previously detailed the different cavitation indexes associated with cavitation regimes. The majority of BBB permeabilization studies perform openings with a fixed acoustic pressure (as well as other sonication parameters) usually predetermined to achieve maximum disruption while yielding minimal vascular damage. Acoustic parameters are typically designed and customized based on the selected animal species, age, and body mass. On the contrary, cavitation control allows the pressure amplitude to be adapted to the animal and to the dynamic behavior of MBs during ultrasound excitation.

Nineteen papers implementing cavitation feedback control were found in the literature, 15 are *in vivo*, four are *in vitro* studies. Some of them were focused on the control algorithm and signal processing, while others investigated early *in vivo* results of feedback control. Two precursors articles will not be described in detail, as they report inertial cavitation control during high intensity focused ultrasound (HIFU) ablation (Hockam *et al.* (Hockham *et al* 2010)) and a cavitation control method requiring a manual intervention (Arvanitis *et al.* (Arvanitis *et al* 2012)). Table 5 summarizes the different studies presented with their main characteristics.

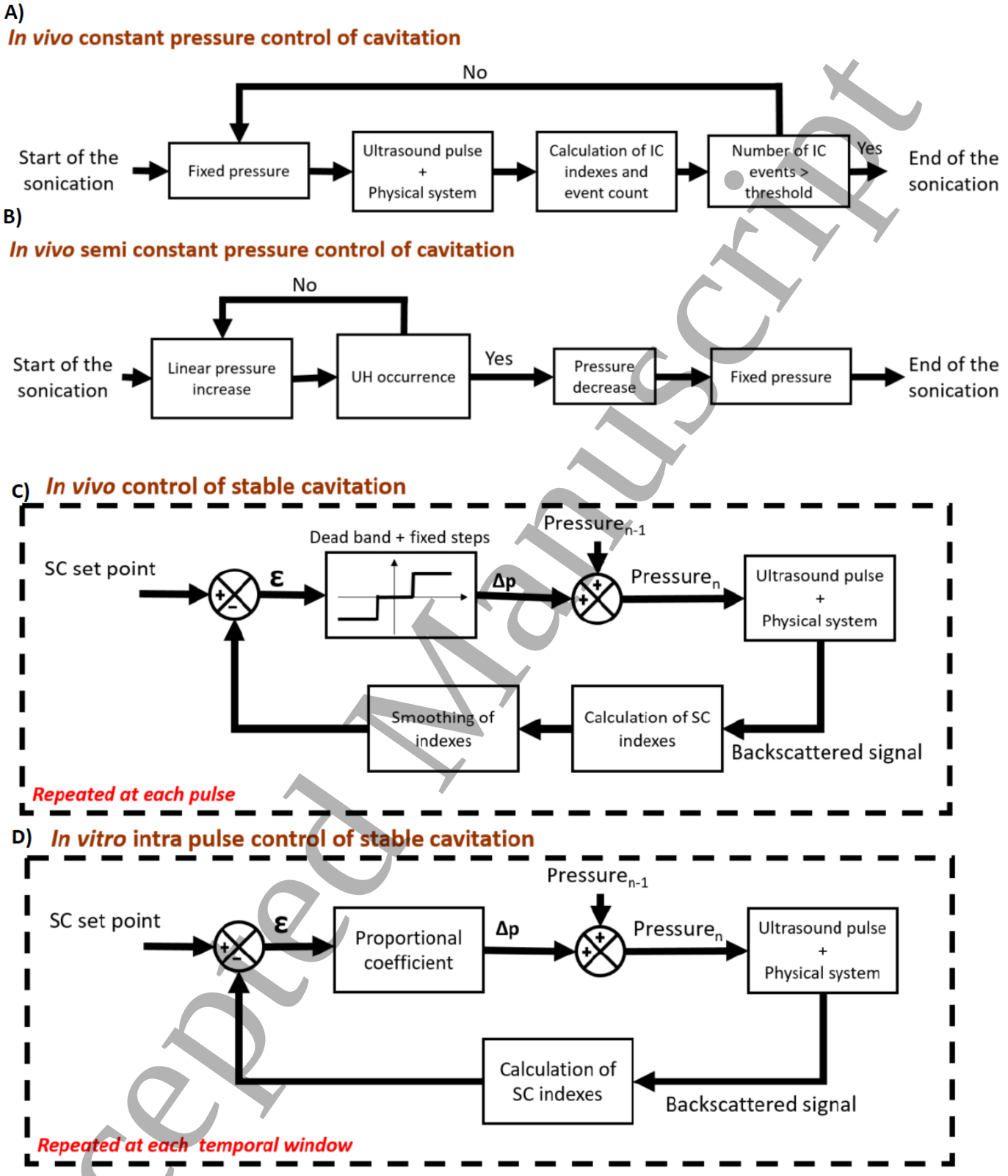

Figure 8: *Examples of 4 different cavitation control algorithms. A) In vivo methods based on the detection of inertial cavitation events*(Huang *et al* 2017) *B) Algorithm used by Toronto university team's*(O'Reilly and Hynynen 2012) *with a semi constant pressure algorithm for in vivo cavitation control. C) Represents the algorithm used in vivo for cavitation control without the ability to change the pressure inside a pulse and the modification to prevent overshoot or*

divergence of the ultrasound pressure. The index n corresponds to the number of the considered pulse(Bing *et al* 2018). *D) Typical intrapulse cavitation control algorithm enabling pressure modulation in vitro. The n value corresponds to the number of the time window of the backscattered signal considered*(Cornu *et al* 2018). *(ε : difference between setpoint and measurement, SC : stable cavitation, IC : inertial cavitation, ΔP : pressure variation)*

3.1 *In vitro* cavitation control

We first focus on cavitation control studies performed *in vitro*. Although these studies avoid the issues related to the biological parameters of the animal, they offer significant technological advances. First, Desjouy *et al.* (Desjouy *et al* 2013) presented an algorithm adjusting the ultrasonic pressure in order to control the inertial cavitation level in water. In this study, it was assumed that the average of the spectral response corresponded to inertial cavitation and harmonics were negligible. An integral controller was used. An integral controller is a controller that will vary the command by a value proportional to the difference between the measurement and the setpoint. The ultrasonic pressure was varied by adding the difference between the measurement signal and the setpoint, multiplied by a coefficient. The pulses lasted 25 ms and the feedback loop lasted 300 µs thanks to the use of Field Programmable Gate Array (FPGA). The MBs were endogenous and must had to be created at the beginning of each pulse. This led to strong oscillations for the first pulses because the cavitation pressure was much higher than the pressure required to maintain inertial cavitation.

In another study, Desjouy's *et al.* (Desjouy *et al* 2015) used 2 separate transducers in transmission and SonoVue® MBs. The use of exogenous MBs showed an improvement in cavitation stability as well as a reduction in ultrasound pressure to reach the same oscillation regime.

The work by Cornu *et al.* (Cornu *et al* 2018) exploited FPGAs for the control of stable cavitation *in vitro*. Interestingly, acoustic pressure was able to vary inside an excitation pulse thanks to the use of FPGA. Experiments were performed in a water tank in which no MB was added. The SH component was extracted from the PCD signal by integrating the spectrum over a frequency band centered on SH to represent stable cavitation. The band noise was also monitored to obtain information on inertial cavitation, but was not used by the feedback control algorithm. The controller was a pure integrator that used the SH component as the input signal. The stable cavitation setpoint was determined from open-loop testing for SC values where no inertial cavitation (IC) was detected. The feedback loop was able to reach a rate control up to 250 µs. The paper showed the possibility of controlling stable cavitation by avoiding inertial cavitation *in vitro*. This algorithm operates in a similar way to the algorithms of Desjouy *et al.* illustrated in Figure 8D.

Patel and co-workers presented an *in vitro* cavitation control method using PAM(Patel *et al* 2018). Cavitation was performed in a tube with MBs flowing through it, all immersed in a tank of water with the ultrasonic transducers. The control signal was the ultrasonic pressure. The backscattered signal was retrieved by an array transducer to perform PAM analysis. The controller was an integral type with a dead band to limit the sensitivity to noise. The dead band is a minimum error value, ε_{min}, necessary to vary the pressure, this means that for a deviation from the set point lower than ε_{min} the ultrasonic pressure is not modified. The controller used the UH components as the error signal. The band noise was also monitored to reduce the ultrasonic pressure by a fixed amount when a substantial increase of noise was noticed (101% compared to baseline). This controller was limited by the computation time of the PAM, therefore its feedback loop lasted 500 ms. Stable cavitation was maintained around the set point during 6s with a tolerance of 10%

3.2 *In vivo* cavitation control with constant pressure

Several studies have focused on keeping the ultrasonic pressure constant while varying the sonication time to control cavitation. These studies require previous experiments on animals of the same characteristics in order to determine precisely the pressure to be applied. These algorithms are therefore generally less robust than those presented in the following section with a pressure adjusted over the treatment.

The article of Tsai *et al.* in 2016(Tsai *et al* 2016) presented PCD cavitation control for a BBB opening on rats. The sonication pressure was kept constant throughout the sonication which ended when the SH component exceeded a threshold (5.5dB increase from the baseline level). This threshold was determined based on preliminary experiments to ensure the best sensitivity and specificity. The control loop was among the slowest (1s). The sonication times related to this control were highly variable. For a pressure of 0.82MPa, one sonication was completed in 5s and another in 40s.

Huang *et al.* (Huang *et al* 2017) published a paper using constant pressure and variable sonication time for BBB opening. It involved the BBB disruption on pigs through fragments of human skulls place on the top of the animal's head. The signal used for this control was obtained by integrating a wide frequency band around the SH component (115+-40 kHz). Two thresholds were defined (0.15 and 0.20, normalized values), and when the calculated index exceeded one of the thresholds, the counter associated with this index was incremented. Counters are emptied at each time period when the threshold is not exceeded. When the number of events associated with one of the counters of SH events exceeded a fixed number (30 for the 0.15 threshold and 3 for the 0.20), the sonication was terminated. The feedback loop had a duration of 30ms. This algorithm is depicted in Figure 8A to illustrate the constant pressure cavitation control algorithms.

The last paper reporting cavitation control with constant pressure was published by Ji and co-workers(Ji *et al* 2021). The cavitation control was used in mice to permeabilize the BBB. However, the focus of this study was to investigate the correlation between markers of inflammation and BBB opening. The control parameters were sonication duration and MBs reinjections. The measured signal was the cavitation dose. It was calculated by integrating the frequency bands (0.2 MHz) around the harmonics, from the third (4.5 MHz) to the ninth (13.5 MHz). A baseline was measured before the MB injection. A cumulative cavitation dose (CCD) was defined. After each pulse, if the measured cavitation dose was lower than the baseline cavitation dose, then MBs were reinjected. When the cumulative dose of all pulses exceeded the total dose set point, the sonication was terminated. In this study 3 different cavitation doses were set:$1 \times 10^7 V^2 s, 5 \times 10^7 V^2 s, 1 \times 10^8 V^2 s$. Although the acoustic pressure was the same for all CCDs, the mice with the lowest dose had no vascular damage, whereas those with the highest CCD had extravasations visible with histology and edemas visible on MRI.

3.3 *In vivo* cavitation control with semi constant pressure

The algorithms described in this section were developed by Hynynen's lab at the University of Toronto to adjust the ultrasound pressure to each experiment. A 2-step algorithm was designed. First, the acoustic pressure linearly increases until the selected UH/SH component emerges from the noise. Then, once the UH threshold is exceeded, the acoustic pressure is reduced to a fixed percentage of its last value. The pressure is then kept constant for the rest of the sonication. This algorithm is illustrated in figure 8B.

The 1st study implementing *in vivo* a feedback control algorithm for MBs cavitation was proposed by O'Reilly and Hynynen in 2012(O'Reilly and Hynynen 2012). This study described ultrasound pressure regulation during FUS-induced BBB opening in rats. This *in vivo* study evaluated the effectiveness of such control on the safety of BBB opening. Pressure control was achieved by monitoring the second and third UH of the backscattered signal using PCD. Once the UH emerged from the noise during the pressure amplitude ramping phase, the pressure was immediately reduced in the next pulse to a fixed percentage (25%, 50% or 75%). Sonication is then pursued at this pressure up to the end. The feedback loop time was 500 ms. The study also showed that this type of sequence was efficient and safe when ultrasound amplitude was decreased to 25% and 50%.

Three other studies confirmed the effectiveness of the protocol while focusing on different other aspects: influence of the bubble type, use of PAM, effectiveness of drugs. The first of these articles was published a few years later by the same group. It described a new device that allowed PAM and thus spatial localization of cavitation (Jones *et al* 2018). Moreover, the emission transducers were able to steer the ultrasonic beam, allowing a displacement of the focal spot. The control index was the SH. However, the control loop had been slowed down (1s). The calculation time of the PAM depended on the field of view (FOV) reconstructed. For a small FOV, the reconstruction time was 85 ms. Authors concluded that, for clinical application, it could be interesting to use a FOV containing the whole skull to detect standing waves. This would increase the calculation time to 27s using their setup.

The second paper was published by McMahon *et al.* (McMahon *et al* 2020). It focused in part on reiterating O'Reilly's 2012 experiment with a comparison between 3 types of MBs: BG8774, Definity and MSB4. The study still used the second and third UH as the measured signal to stop the ultrasound pressure increased. The pressure was only reduced by 50% at the onset of the ultra-harmonics. The ultra-harmonics were considered to have occurred when their value exceeded by 10 standard deviations of the UH baseline value. The study confirmed the absence of damage observed by extravasation of red blood cells 7 days after sonication although some extravasations were observed 24 hours after sonication. No significant difference was found between the different MBs for feedback control.

The last article using this protocol was published by Lynch *et al*.(Lynch *et al* 2021). The frequency bands observed were this time the UH at $1.5f_0$, 2.5 f_0, and 3.5 f_0. The amplitude of the ultrasonic pressure emitted by the transducer was reduced by 75% when the UH emerged from the band noise. This control was used in this study to evaluate the reclosure time of the BBB after FUS-induced BBB disruption and administration of vasculotide. The conclusion of the study was that vasculotide accelerates BBB restoration after permeabilization in the presence of amyeloid pathology.

3.4 *In vivo* cavitation control with variable pressure

Within this section, we report *in vivo* studies that focused on cavitation control by variation of the ultrasonic pressure applied during sonication. The main difference from those reported in the previous section is the upward and downward variation of the ultrasonic pressure.

Kamimura *et al.* (Kamimura *et al* 2019) opened the BBB in NHP using a protocol that controlled the increase of acoustic pressure with a stepwise method. The measurement signal was an inertial cavitation index. This index was calculated by integrating the spectrum of the backscattered signal from MBs outside the frequency bands surrounding the harmonics and UH. An event occurred if the IC index exceeded a threshold (150% of the baseline value) during a pulse. The control algorithm included a ramp phase during which the pressure was increased with each pulse by a fixed pressure

step of 9kPa. The increase can be paused and the pressure was decreased by the same step as soon as an event occurred but the ramp would re-start the increase in the following pulse. The ramping phase ended only if 2 events occurred in the last second (*i.e.,* in the 5 last pulses) or if the number of event is superior to ten. The pressure was then kept constant and decreased by a fixed pressure step of 9kPa if 2 new consecutive events occurred. The IC threshold was chosen on the basis of previous experiments. This study showed the robustness of this algorithm to open the BBB while avoiding any vascular damage.

The exact same protocol as in Kamimura's article was repeated in the article published by Novell *et al.* (Novell *et al* 2020). Data from PCD records were used to propose a new cavitation index to prevent vascular damage. This new cavitation index could only be used if the loop times fall below the pulse duration in order to allow for pressure modulation within a pulse. The evolution of UH was observed inside a pulse (typically 10 ms) to observe the destabilization of the MBs over time. The UH level was compared to a reference window at the beginning of this pulse. The UH appeared spontaneously before the inertial cavitation onset (in less than 128 µs). The objective is to stop the excitation pulse or reduce its amplitude as soon as the UH content is detected, allowing for an immediate reaction.

A study published by Sun and co-workers in 2017(Sun *et al* 2017) used a more complex protocol for BBB opening in rats. Sonication time and ultrasonic amplitude were both variable. The indexes calculated from the backscattered signal were the harmonic components (stable CCD) and the broadband noise (IC). The pressure amplitude was controlled by an integral controller to reach a target setpoint on the harmonic component. The set point was chosen from a previous study and was defined as the point below the maximum value of the harmonic component reached without any simultaneous increase of the broadband noise. The stable CCD was calculated by integrating and summing all harmonic emissions of each pulse. Once the selected CCD was reached, the sonication was terminated. A safety condition was also implemented in the feedback control: if an increase of the broadband noise emissions was detected, the emitted pressure was reduced in the following pulse by a fixed step. The feedback loop lasted 250ms and the authors agreed that one of the best ways to improve the safety of the sonication was to reduce this duration.

Bing *et al.* published in 2018(Bing *et al* 2018) a study comparing 3 different types of MBs (Definity, Optison, homemade nanobubbles) for BBB opening in rats. The measurement signal was an index calculated from the frequency decomposition of the backscattered signal for an entire pulse. The index was calculated by integrating the second UH component (0.75 MHz) on a frequency band (±0.05 MHz), this value was averaged with the value of the 2 previous pulses. The set point was chosen from previous studies of BBB opening. The control was based on a fixed pressure variation (10 to 30 kPa) depending on whether the index was superior or inferior to a dead band surrounding the setpoint. The feedback loop lasted 1 second. This was an efficient solution to adapt an integral control when the refresh rate of the algorithm was slower than the system to be controlled. This algorithm is represented in figure 8C with integral controller for a control carried out pulse to pulse.

Çavuşoğlu and co-workers then published an article(Çavuşoğlu *et al* 2019) on cavitation control in mice focusing on the differentiation between oscillation regimes of MBs. The control was achieved by a pulse-to-pulse variation of the ultrasound pressure. The measurement signal was the IC index which was calculated from the integral of the spectrum outside the frequency bands (+-150 kHz) surrounding the harmonic and UH components. Their control was based on a pre-calibration in 2 steps. A first pre-calibration of 20 minutes was performed by applying multiple pressure levels on different animals perfused with a MBs solution. Then the treated animals underwent a 80s pre-calibration step which consisted in applying the same pressure levels as for the calibration animals. In this pre-

calibration step, pulses lasted only 200µs as a safety measurement and was used to establish relationships with the pre-calibration bands of the first experiment in order to reduce the effect on inter-animal variations. The control was performed by determining from the IC index values of the previous pulses, the corresponding cavitation states from the different oscillation modes obtained with the pre-calibration. The ultrasonic pressure of the next pulse was then chosen to be as close as possible to the SC state. Despite a slow control loop (1s), the control was effective. However, pre-calibration appeared to cause some extravasation of red blood cells.

A recent article published by McDannold *et al.* in 2020(McDannold *et al* 2020) presented a cavitation control in rats based on an ultrasound pressure control. The feedback control only lasted a few seconds and then the average pressure value of the initial step was maintained for the rest of the sonication. The index used to measure the state of cavitation was the integral of the spectrum surrounding the second and third harmonics (460 and 690 ± 10 kHz). The integral controller increased or decreased the pressure by a value proportional to the difference between the setpoint and the index value. A dead band was implemented around the setpoint to limit the sensitivity to noise. The control started at the 8th second, it stopped at the 30th second, the average value of the pressure during the control was then fixed for the remaining 25s. The pressure could still be reduced if the SH component emerged from the noise or if the band noise exceeded a certain threshold. The study concluded that it was possible to open the BBB repeatedly and without damage with the ExAblate clinical system. The pulse repetition frequency was 1.1Hz .

Chien and co-workers published a study (Chien *et al* 2022b)on BBB opening in mice. The measurement signal was the third harmonic of the backscattered spectrum representing SC. A baseline was previously acquired for 10 pulses after the MBs infusion was started at relatively low pressure (0.2MPa). The purpose of the cavitation control was to obtain different increases of the SC with respect to the baseline (0.5, 1, 2, 3, 4 dB). After an initial phase of linear pressure increase, the SC was maintained by varying the ultrasonic pressure by a fixed step (13kPa) when the deviation between SC and setpoint exceeded a certain threshold. The loop duration was 500ms. For each setpoint, BBB opening volume and histological damage were described. All the set points allowed BBB permeabilization and the setpoints (0.5, 1, 2 dB) did not induce detectable ERBC.

Another study was then published by Chien and co-workers (Chien *et al* 2022a), using the same protocol. This time the study was performed on pigs as a large animal model. The baseline was composed of only 5 pulses that were shot at a pressure of 0.3MPa. The setpoints were (0.25, 0.5, 1 dB). All 3 setpoints resulted in BBB opening and only the 1dB setpoint resulted in visible histological damage. The loop time was slowed to 1s.

An article published by Lee et al. (Lee *et al* 2022) presents BBB opening in mice with the objective of promoting the proinflammatory marker ICAM-1 and delivering anti-PD1 in a mouse model of glioblastoma. The control strategy implemented aimed to achieve a target increase in the stable cavitation index. This index was calculated by integrating the third harmonic of the backscattered signal. The pressure was then adjusted to reach the setpoint for stable cavitation. A behavior law for the emissions of the third harmonic was constructed based on previous data. The step size varied according to the proximity between the collected data and the reconstructed model. The model itself was fitted onto the pressure-amplitude relationship using a hyperbolic tangent model. Furthermore, this controller was activated only after the detection of the MB bolus in the bloodstream and was terminated after a 20% decrease in MB concentration. A safety measure was implemented by monitoring the broadband noise, where the pressure was automatically reduced by a fixed step upon detection. The control loop had a duration of 1 second. The control approach proved to be effective, safe, and robust against biological variations in all tested mice.

Study	Model	Microbubbles concentration injection	Control Loop Frequency	Control strategy	Pressure control	Sonication termination	Use of baseline	Safety control
Desjouy(Desjouy *et al* 2013)	*in vitro*	Endogenous N/A N/A	3,3 kHz	Integral	Closed-loop (Broadband noise (BB))	End of duration	No	No
Desjouy(Desjouy *et al* 2015)	*in vitro*	SonoVue $2.5\ 10^6$ MB/mL N/A	3,3 kHz	Integral	Closed-loop (Broadband noise)	End of duration	No	No
Cornu(Cornu *et al* 2018)	*in vitro*	Endogenous N/A N/A	4 kHz	Integral	Closed-loop (Sub-harmonics)	End of duration	No	No
Patel(Patel *et al* 2018)	*in vitro*	Optison $6\ 10^3$Mb/mL infusion	2 Hz	Integral	Closed-loop (Ultra-harmonics)	End of duration	No	Fixed pressure step (BB)
Tsai(Tsai *et al* 2016)	rats	SonoVue 100 µL/kg bolus	1 Hz	Threshold Based	Open-loop	Sub-harmonics dose	Yes	Stop with sub-harmonics dose
Huang(Huang *et al* 2017)	pigs	Definity 10 - 20 µL/kg bolus	33 Hz	Threshold Based	Open-loop	Sub-harmonics events	Yes	Stop with sub-harmonics dose
Ji(Ji *et al* 2021)	mice	Definity 100 µL/kg bolus	2 Hz	Threshold Based	Open-loop	Harmonic dose	Yes	No
O'reilly(O'Reilly and Hynynen 2012)	rats	Definity 20 µL/kg infusion	2 Hz	Threshold Based	Open-loop (Ultra-harmonic)	End of duration	Yes	No
Jones(Jones *et al* 2018)	rabbits	Definity 200 µL/kg infusion	11.8 Hz	Threshold Based	Open-loop (Broadband noise)	End of duration	Yes	No
McMahon(McMahon *et al* 2020)	rats	BG8774, Definity, MSB4 500 µL/kg infusion	2 Hz	Threshold Based	Open-loop (Ultra-harmonic)	End of duration	Yes	No
Lynch(Lynch *et al* 2021)	mice	Definity 20 µL/kg bolus	1 Hz	Threshold Based	Open-loop (Ultra-harmonic)	End of duration	No	No
Kamimura(Kamimura *et al* 2019)	macaques	SonoVue 300 µL/kg bolus	5 Hz	Threshold Based	Open-loop (Broadband)	End of duration	Yes	Fixed pressure step (BB)
Novell(Novell *et al* 2020)	rats, macaques	SonoVue 300 µL/kg bolus	10 Hz	Threshold Based	Open-loop (Broadband noise)	End of duration	Yes	Fixed pressure step (BB)
Sun(Sun *et al* 2017)	rats	Optison 10 µL/kg	4 Hz	Integral	Closed-loop (sub-harmonics)	Harmonics dose	No	Fixed pressure step (BB)

		bolus+infusion						
Bing(Bing *et al* 2018)	rats	Definity, Optison, HM 1.1–1.2 µl/ml* infusion	1 Hz	Fixed pressure step (dead band)	Closed-loop (Ultra-harmonics)	End of duration	Yes	No
Çavuşoğlu(Çavuşoğlu *et al* 2019)	mice	BG8235 10 µL/kg infusion	1 Hz	Variable step	Closed-loop (Broadband noise)	End of duration	Yes	No
McDannold(McDannold *et al* 2020)	rats	Definity 10 µL/kg bolus	1.1 Hz	Integral for ⅓ then fixed pressure	Closed-loop (Harmonics)	End of duration	Yes	Fixed pressure step (BB or subharmonics)
Chien(Chien *et al* 2022b)	mice	Definity 1.2 µL/kg infusion	2 Hz	Fixed pressure step (dead band)	Closed-loop (Harmonics)	End of duration	Yes	No
Chien(Chien *et al* 2022a)	pigs	Definity 10 µL/kg infusion	1 Hz	Fixed pressure step (dead band)	Closed-loop (Harmonics)	End of duration	Yes	No
Lee(Lee *et al* 2022)	mice	Definity 100 µL/kg bolus	1Hz	Integral with variable step	Closed-loop (Harmonics)	End of duration	Yes	Fixed pressure step (BB)

Table 5: *Table summarizing the different characteristics of feedback control algorithms. The in vitro algorithms (3.1) are identified in blue, the in vivo constant pressure algorithms (3.2) are identified in orange, the in vivo semi-constant pressure algorithms (3.3) are identified in grey and the in vivo variable pressure algorithms (3.4) in green. The "control strategy" specifies whether the algorithm uses an integral controller, a control based on threshold detection or fixed step variation with a dead band to vary the pressure. The column "pressure control" specifies if the pressure is in open-loop, in closed-loop with in brackets the type of frequency component used as a measurement signal. The algorithms in open-loop with a component in brackets indicate for the algorithms with semi-constant pressure the component whose detection makes it possible to switch from a pressure ramp to a fixed pressure. The column "safety control" specifies if a control of the inertial cavitation allows a protective behavior of the algorithm by decreasing the pressure by a fixed step from a too important component (between parentheses) or the termination of the sonication from the total inertial cavitation dose exceeding a threshold. (*This concentration is expressed in volume of gas/ volume of injected liquid) Additional data can be found in S8 Table.*

Discussion

The studies presented in the third section illustrate the importance of controlling cavitation in real-time *in vivo*. The sections 2.5, 2.6 and 2.7 highlight the wide variety of cavitation indexes and baselines that have been used, as well as the different methods for calculating them. We pointed out some substantial differences in cavitation monitoring strategies used by the research groups, partly due to disparities in equipment, animals and experimental setups used (*e.g.*, lower frequencies for thicker skulls, see Table 1). There are also differences in the interpretation of certain frequency components. Broadband noise is commonly measured to predict potential hemorrhage or edema, its

biological impact being consensual. The harmonics represent only the stable cavitation when monitored and interpreted. Regarding UH and SH, several conclusions exist. Some studies will consider UH/SH components as stable cavitation while others will consider them as broadband noise. This has an impact on the cavitation control algorithms, which are then going to have different functioning in the use of the UH/SH whether they are interpreted as stable or inertial cavitation.

The *in vivo* studies have set up protocols to run safe pulse-to-pulse control with loop times longer than 10 ms. The main concern with current control algorithms is the processing delay. Indeed, it is challenging to preserve stable and efficient cavitation over a pulse as the dynamic behavior and the concentration of MBs vary over time. The extreme variability of MBs response is best illustrated by all BBB permeabilization studies at constant ultrasonic pressure where stable or inertial cavitation indexes can vary by a factor of 10 for consecutive pulses. Therefore, even for successive shots of similar amplitude and duration, the variable flow of polydisperse MBs in the ultrasonic beam will generate different cavitation responses (stochastic phenomenon). Therefore, the lack of control within a pulse requires great care to be taken (*i.e.*, using safety margins at the expense of efficacy) to avoid the occurrence of inertial cavitation. All algorithms evaluated in *in vivo* studies are the result of very safe strategies: highly progressive increase, reduction of amplitude at the onset of IC. As some studies have pointed out(Novell *et al* 2020), it is possible at the beginning of some pulses to detect the IC very early. This detection in real-time would allow a reduction of the amplitude or the termination of the pulse. This simple implementation could strongly reduce the duration of IC within a pulse (down to 250µs with FPGAs implementation). The *in vitro* studies use mostly algorithms with intrapulse controls. These studies allow us to observe the types of algorithms, mostly integral controllers that can be used *in vivo* once FPGA technologies are implemented. Currently, only a few groups have the means to implement such control, while many prefer to focus on the pharmaceutical and biological aspects, opting for pulse-to-pulse control.

The literature review presents *in vitro* studies with different types of control adapted to very short loop times. The results obtained *in vitro* benefit from a focal spot without aberration and a more intense backscattered signal. Recently, first examples of the use of FPGAs in intrapulse cavitation control have been performed *in vivo* with a transmission study through a skull(Cornu *et al* 2022).

The duration of sonication required to open the BBB is highly variable. Most studies use sonications that last between 2 and 3 minutes, *i.e.*, until MBs are eliminated from the bloodstream. However, other studies achieve BBB permeabilization with sonications of less than 10s(Tsai *et al* 2016). Likewise, many other parameters are fixed in cavitation control studies: type of MBs used, pulse repetition frequency, pulse duration, MB injection method. Each group has optimized these parameters, but differences in the protocol can result in major discrepancies in the results and make the comparison between strategies very complex. Thus, each combination of species, PCDs, emitters, MBs could have a dedicated algorithm and ultrasound parameters to optimize BBB permeabilization efficiency and safety process.

Concerning the use of different cavitation indexes, we could summarize that two distinct indexes are needed. The first one would be a stable cavitation index and thus an index correlated to the permeabilization of the BBB. It could be obtained it from the harmonic components and it would have to be maximize. The second would be a hazard index, which would be an indicator of inertial cavitation and that should therefore be minimized. This index could probably be calculated from broadband noise. The destabilization of MBs calculated from the ultraharmonic components of MBs could also be included in this hazard index. This would allow to prevent the onset of vascular damage resulting from inertial cavitation at an earlier stage.

Despite numerous proofs of concept and preclinical studies, few clinical trials on BBB permeabilization have been completed in humans. To date, recruiting is underway for several clinical studies (Beccaria *et al* 2020, Bunevicius *et al* 2020, Chen *et al* 2021b). The different pathologies targeted by these studies are glioblastoma, Alzheimer's disease, Parkinson's disease and amyotrophic lateral sclerosis. Several teams use different systems to achieve BBB permeabilization in the human brain(Chen *et al* 2021a, Mainprize *et al* 2019a, Wu *et al* 2018a, Beccaria *et al* 2013).

The various articles (Abrahao *et al* 2019, Gasca-Salas *et al* 2021, Mainprize *et al* 2019b, Pavlos Anastasiadis *et al* 2021, Lipsman *et al* 2018) reporting on clinical protocols for BBB opening with cavitation control all employ the same pressure control protocol and system, namely, amplitude reduction following detection of the subharmonic component using the Exablate system. Another study by Huang (Huang *et al* 2022) implemented a different cavitation control algorithm, using a ramped pressure approach until reaching the desired subharmonic value, which was then maintained at a constant pressure. The findings are preliminary but promising, demonstrating successful BBB disruptions without any observed negative side effects. In the future, we anticipate the publication of additional treatment outcomes associated with BBBO, as well as the emergence of various BBB control techniques. However, the implementation of these techniques may be subject to delays due to country-specific regulations governing the testing of new ultrasound protocols.

The dose of cavitation exposure in the context of BBB opening and its correlation with drug delivery has emerged as a new area of investigation that is receiving significant attention within the research community. This is particularly relevant given the surge in studies examining the effectiveness of different drugs. Recent research has established correlations between the dose of cavitation and the amount of drugs delivered(Ji *et al* 2021, Lee *et al* 2023, Chen and Konofagou 2014, Marquet *et al* 2014, Wu *et al* 2014), highlighting the potential for optimizing drug delivery to the brain through feedback loops based on these dose-response relationships. Exploring the dose of cavitation and its correlation with drug delivery presents a promising avenue for enhancing the efficiency and precision of drug delivery across the BBB. The use of algorithms informed by these correlations offers new possibilities for optimizing targeted drug delivery to the brain.

Achieving BBB opening over a volume also represents a major challenge. While most studies in rodents are limited to opening a focal spot, observations in clinical studies have shown different volume openings using electronic steering and a series of juxtaposed shots. However, there are no articles currently available on BBB opening with ultrasound pressure control using a moving transducer. In clinical studies, the permeabilization volumes are significantly larger than in preclinical studies, necessitating further research in this area. By utilizing mechanical transducer displacement, it would be possible to maintain a constant PRF while scanning across multiple volumes, specifically targeting the regions of interest for treatment. This approach enables continuous firing, creating the desired PRF excitation specifically in the cerebral parts of the volume that require intervention. As a result, treatment efficiency is improved, and the lifespan of MBs is optimized for volumetric openings.

In the context of BBB opening *in vivo*, the absence of a comprehensive model to simulate the obtained results poses a significant challenge. While it is feasible to model the interactions between a finite number of MBs, the polydispersed nature of the MBs, along with their varying positions and proximity to the blood capillary walls, which themselves exhibit diverse positions, sizes, and orientations, make it extremely challenging to simulate the entirety of these complex interactions. However, with advancements in computational power and ongoing developments in this field, the potential for utilizing simulations to estimate certain parameters and potentially reducing the number of experiments exists. These advancements offer promising avenues for future research and exploration.

Furthermore, alongside these advancements, the growing utilization of PAM holds great potential in addressing the challenges of BBB opening. PAM enables the confirmation of the precise position of cavitation zones. This technology offers the advantage of limiting positioning errors and preventing unintended cavitation outside the targeted permeabilization zone. By incorporating a feedback loop based on electronic steering or mechanical displacement, it becomes possible to minimize errors in focal spot positioning, ultimately eliminating the reliance on MRI for treatment guidance. This integration of PAM and real-time feedback mechanisms represents a significant step towards enhancing the precision and effectiveness of BBB opening procedures.

Finally, artificial intelligence (AI) and machine learning techniques have the potential to optimize focused ultrasound-mediated BBB opening procedures, taking them to the next level. Lee et al. (Lee *et al* 2023) recently demonstrated the successful application of deep learning algorithms to detect BBB opening volumes, resulting in reduced doses of injected contrast agents for MRI. However, it should be noted that the effectiveness of these AI methods in enhancing cavitation control is contingent upon the availability of extensive human data for training. Additionally, AI algorithms, such as those studied by Xu et al. (Xu *et al* 2019a), show promise in improving the detection and classification of cavitation states. Integrating AI and machine learning methods, informed by well-developed physical models and extensive human data, holds the potential to enhance the precision and efficiency of BBB opening procedures, enabling personalized and optimized drug delivery to the brain.

Conclusion

In conclusion, this review has highlighted the significant progress that has been made in the understanding of cavitation control and its impact on BBB permeabilization. However, several challenges remain to be addressed, including the stochastic nature of cavitation and the need for individualized pressure control for diverse microbubble populations. Further investigation is needed to translate preclinical findings into clinical settings, with a specific focus on scaling up permeabilization volumes and implementing ultrasound pressure control through human skulls. Addressing these challenges is essential to explore the full potential of microbubble-mediated BBB opening as an efficient therapeutic strategy for various cerebral diseases.

Funding: This work was funded by the CAMI Labex (ANR-11-LABX-0004-01)

Conflicts of Interest: The authors declare no conflict of interest.

Abbreviations

UH : Ultraharmonic

SH : Subharmonic

MB : Microbubble

BBB : Blood-Brain Barrier

FUS : Focused Ultrasound

NHP : Non Human Primate

FFT : Fast Fourier Transform

PCD : Passive Cavitation Detection

PRF : Pulse repetition frequency

FPGA : Field Programmable Gate Array

ERBC : Extravasated Red Blood Cells

MRI : Magnetic Resonance Imaging

CCD : Cumulative Cavitation Dose

PAM : Passive Acoustic Mapping

Hz : Hertz

Pa : Pascal

BB : Broadband

IC : Inertial Cavitation

SC : Stable Cavitation

References:

Abrahao A, Meng Y, Llinas M, Huang Y, Hamani C, Mainprize T, Aubert I, Heyn C, Black S E, Hynynen K, Lipsman N and Zinman L 2019 First-in-human trial of blood-brain barrier opening in amyotrophic lateral sclerosis using MR-guided focused ultrasound *Nat Commun* **10** 4373

Angla C, Larrat B, Gennisson J-L and Chatillon S 2023 Transcranial ultrasound simulations: A review *Med Phys* **50** 1051–72

Apfel R E 1982 Acoustic cavitation: a possible consequence of biomedical uses of ultrasound. *Br J Cancer Suppl* **5** 140–6

Arvanitis C D, Livingstone M S and McDannold N 2013 Combined ultrasound and MR imaging to guide focused ultrasound therapies in the brain *Physics in Medicine and Biology* **58** 4749–61

Arvanitis C D, Livingstone M S, Vykhodtseva N and McDannold N 2012 Controlled Ultrasound-Induced Blood-Brain Barrier Disruption Using Passive Acoustic Emissions Monitoring ed A Muñoz-Barrutia *PLoS ONE* **7** e45783

Arvanitis C D, Vykhodtseva N, Jolesz F, Livingstone M and McDannold N 2016 Cavitation-enhanced nonthermal ablation in deep brain targets: feasibility in a large animal model *Journal of Neurosurgery* **124** 1450–9

Aryal M, Fischer K, Gentile C, Gitto S, Zhang Y-Z and McDannold N 2017 Effects on P-Glycoprotein Expression after Blood-Brain Barrier Disruption Using Focused Ultrasound and Microbubbles *PLoS One* **12** e0166061

Asahara M 2013 Shape variation in the skull and lower carnassial in a wild population of raccoon dog (Nyctereutes procyonoides) *Zoolog Sci* **30** 205–10

Asquier N, Chapelon J-Y and Lafon C 2020 Evaluation of the Uncertainty of Passive Cavitation Measurements for Blood–Brain Barrier Disruption Monitoring *Ultrasound in Medicine & Biology* **46** 2736–43

Bader K B, Gruber M J and Holland C K 2015 Shaken and stirred: mechanisms of ultrasound-enhanced thrombolysis *Ultrasound in Medicine & Biology* **41** 187–96

Bader K B, Vlaisavljevich E and Maxwell A D 2019 For Whom the Bubble Grows: Physical Principles of Bubble Nucleation and Dynamics in Histotripsy Ultrasound Therapy *Ultrasound Med Biol* **45** 1056–80

Barzegar-Fallah A, Gandhi K, Rizwan S B, Slatter T L and Reynolds J N J 2022 Harnessing Ultrasound for Targeting Drug Delivery to the Brain and Breaching the Blood-Brain Tumour Barrier *Pharmaceutics* **14** 2231

Baseri B, Choi J J, Tung Y-S and Konofagou E E 2010 Multi-modality safety assessment of blood-brain barrier opening using focused ultrasound and definity microbubbles: a short-term study *Ultrasound Med Biol* **36** 1445–59

Beccaria K, Canney M, Bouchoux G, Desseaux C, Grill J, Heimberger A B and Carpentier A 2020 Ultrasound-induced blood-brain barrier disruption for the treatment of gliomas and other primary CNS tumors *Cancer Lett* **479** 13–22

Beccaria K, Canney M, Goldwirt L, Fernandez C, Adam C, Piquet J, Autret G, Clément O, Lafon C, Chapelon J-Y and Carpentier A 2013 Opening of the blood-brain barrier with an unfocused ultrasound device in rabbits *J Neurosurg* **119** 887–98

Biagi E, Breschi L, Vannacci E and Masotti L 2007 Stable and transient subharmonic emissions from isolated contrast agent microbubbles *IEEE Trans Ultrason Ferroelectr Freq Control* **54** 480–97

Bing C, Hong Y, Hernandez C, Rich M, Cheng B, Munaweera I, Szczepanski D, Xi Y, Bolding M, Exner A and Chopra R 2018 Characterization of different bubble formulations for blood-brain barrier opening using a focused ultrasound system with acoustic feedback control *Scientific Reports* **8** 7986

Blake J R and Gibson D C 1987 Cavitation Bubbles Near Boundaries *Annual Review of Fluid Mechanics* **19** 99–123

Boulos P, Varray F, Poizat A, Ramalli A, Gilles B, Bera J-C and Cachard C 2018 Weighting the Passive Acoustic Mapping Technique With the Phase Coherence Factor for Passive Ultrasound Imaging of Ultrasound-Induced Cavitation *IEEE transactions on ultrasonics, ferroelectrics, and frequency control* **65** 2301–10

Bunevicius A, McDannold N J and Golby A J 2020 Focused Ultrasound Strategies for Brain Tumor Therapy *Oper Neurosurg (Hagerstown)* **19** 9–18

Burgess M T, Apostolakis I and Konofagou E E 2018 Power cavitation-guided blood-brain barrier opening with focused ultrasound and microbubbles *Physics in Medicine and Biology* **63** 065009

Cammalleri A, Croce P, Lee W, Yoon K and Yoo S-S 2020 Therapeutic Potentials of Localized Blood-Brain Barrier Disruption by Noninvasive Transcranial Focused Ultrasound: A Technical Review *Journal of Clinical Neurophysiology: Official Publication of the American Electroencephalographic Society* **37** 104–17

Çavuşoğlu M, Zhang J, Ielacqua G D, Pellegrini G, Signorell R D, Papachristodoulou A, Brambilla D, Roth P, Weller M, Rudin M, Martin E, Leroux J-C and Werner B 2019 Closed-loop cavitation control for focused ultrasound-mediated blood-brain barrier opening by long-circulating microbubbles *Physics in Medicine and Biology* **64** 045012

Chapelon J Y, Cathignol D, Cain C, Ebbini E, Kluiwstra J U, Sapozhnikov O A, Fleury G, Berriet R, Chupin L and Guey J L 2000 New piezoelectric transducers for therapeutic ultrasound *Ultrasound Med Biol* **26** 153–9

Chen H and Konofagou E E 2014 The size of blood-brain barrier opening induced by focused ultrasound is dictated by the acoustic pressure *Journal of Cerebral Blood Flow and Metabolism: Official Journal of the International Society of Cerebral Blood Flow and Metabolism* **34** 1197–204

Chen K-T, Chai W-Y, Lin Y-J, Lin C-J, Chen P-Y, Tsai H-C, Huang C-Y, Kuo J S, Liu H-L and Wei K-C 2021a Neuronavigation-guided focused ultrasound for transcranial blood-brain barrier opening and immunostimulation in brain tumors *Sci Adv* **7** eabd0772

Chen K-T, Wei K-C and Liu H-L 2021b Focused Ultrasound Combined with Microbubbles in Central Nervous System Applications *Pharmaceutics* **13** 1084

Chen W-S, Brayman A A, Matula T J and Crum L A 2003 Inertial cavitation dose and hemolysis produced in vitro with or without Optison® *Ultrasound in Medicine & Biology* **29** 725–37

Cheng M, Li F, Han T, Yu A C H and Qin P 2019 Effects of ultrasound pulse parameters on cavitation properties of flowing microbubbles under physiologically relevant conditions *Ultrasonics Sonochemistry* **52** 512–21

Chien C-Y, Xu L, Pacia C P, Yue Y and Chen H 2022a Blood–brain barrier opening in a large animal model using closed-loop microbubble cavitation-based feedback control of focused ultrasound sonication *Sci Rep* **12** 16147

Chien C-Y, Yang Y, Gong Y, Yue Y and Chen H 2022b Blood-Brain Barrier Opening by Individualized Closed-Loop Feedback Control of Focused Ultrasound *BME Frontiers* **2022** Online: https://spj.sciencemag.org/journals/bmef/2022/9867230/

Chitnis P V, Farny C H and Roy R A 2019 SVD-Based Separation of Stable and Inertial Cavitation Signals Applied to Passive Cavitation Mapping During HIFU *IEEE Trans Ultrason Ferroelectr Freq Control* **66** 857–66

Chu P-C, Chai W-Y, Tsai C-H, Kang S-T, Yeh C-K and Liu H-L 2016 Focused Ultrasound-Induced Blood-Brain Barrier Opening: Association with Mechanical Index and Cavitation Index Analyzed by Dynamic Contrast-Enhanced Magnetic-Resonance Imaging *Scientific Reports* **6** 33264

Constans C, Ahnine H, Santin M, Lehericy S, Tanter M, Pouget P and Aubry J-F 2020 Non-invasive ultrasonic modulation of visual evoked response by GABA delivery through the blood brain barrier *J Control Release* **318** 223–31

Conti A, Geffroy F, Kamimura H A S, Novell A, Tournier N, Mériaux S and Larrat B 2022 Regulation of P-glycoprotein and Breast Cancer Resistance Protein Expression Induced by Focused Ultrasound-Mediated Blood-Brain Barrier Disruption: A Pilot Study *Int J Mol Sci* **23** 15488

Cornu C, Guédra M, Béra J-C, Liu H-L, Chen W-S and Inserra C 2018 Ultrafast monitoring and control of subharmonic emissions of an unseeded bubble cloud during pulsed sonication *Ultrasonics Sonochemistry* **42** 697–703

Cornu C, Novell A, Selingue E, Mondou P, Agou P, Mériaux S and Larrat B 2022 Ultrafast Intrapulse Feedback Control of FUS-induced BBB Disruption ISTU (Toronto)

Coussios C C and Roy R A 2008 Applications of Acoustics and Cavitation to Noninvasive Therapy and Drug Delivery *Annu. Rev. Fluid Mech.* **40** 395–420

Dauba A, Delalande A, Kamimura H A S, Conti A, Larrat B, Tsapis N and Novell A 2020a Recent Advances on Ultrasound Contrast Agents for Blood-Brain Barrier Opening with Focused Ultrasound *Pharmaceutics* **12** 1125

Dauba A, Goulas J, Colin L, Jourdain L, Larrat B, Gennisson J-L, Certon D and Novell A 2020b Evaluation of capacitive micromachined ultrasonic transducers for passive monitoring of microbubble-assisted ultrasound therapies *The Journal of the Acoustical Society of America* **148** 2248–55

Deffieux T and Konofagou E E 2010 Numerical study of a simple transcranial focused ultrasound system applied to blood-brain barrier opening *IEEE Trans Ultrason Ferroelectr Freq Control* **57** 2637–53

Delalande A, Kotopoulis S, Postema M, Midoux P and Pichon C 2013 Sonoporation: mechanistic insights and ongoing challenges for gene transfer *Gene* **525** 191–9

Desjouy C, Fouqueray M, Lo C W, Muleki Seya P, Lee J L, Bera J C, Chen W S and Inserra C 2015 Counterbalancing the use of ultrasound contrast agents by a cavitation-regulated system *Ultrason Sonochem* **26** 163–8

Desjouy C, Poizat A, Gilles B, Inserra C and Bera J-C 2013 Control of inertial acoustic cavitation in pulsed sonication using a real-time feedback loop system *The Journal of the Acoustical Society of America* **134** 1640–6

Everbach E C, Makin I Raj S, Azadniv M and Meltzer R S 1997 Correlation of ultrasound-induced hemolysis with cavitation detector output in vitro *Ultrasound in Medicine & Biology* **23** 619–24

Fan C-H, Liu H-L, Ting C-Y, Lee Y-H, Huang C-Y, Ma Y-J, Wei K-C, Yen T-C and Yeh C-K 2014 Submicron-bubble-enhanced focused ultrasound for blood-brain barrier disruption and improved CNS drug delivery *PloS One* **9** e96327

Fan C-H, Ting C-Y, Chang Y-C, Wei K-C, Liu H-L and Yeh C-K 2015 Drug-loaded bubbles with matched focused ultrasound excitation for concurrent blood-brain barrier opening and brain-tumor drug delivery *Acta Biomaterialia* **15** 89–101

Felix M-S, Borloz E, Metwally K, Dauba A, Larrat B, Matagne V, Ehinger Y, Villard L, Novell A, Mensah S and Roux J-C 2021 Ultrasound-Mediated Blood-Brain Barrier Opening Improves Whole Brain Gene Delivery in Mice *Pharmaceutics* **13** 1245

Foster F S, Harasiewicz K A and Sherar M D 2000 A history of medical and biological imaging with polyvinylidene fluoride (PVDF) transducers *IEEE Trans Ultrason Ferroelectr Freq Control* **47** 1363–71

Gasca-Salas C, Fernández-Rodríguez B, Pineda-Pardo J A, Rodríguez-Rojas R, Obeso I, Hernández-Fernández F, Del Álamo M, Mata D, Guida P, Ordás-Bandera C, Montero-Roblas J I, Martínez-Fernández R, Foffani G, Rachmilevitch I and Obeso J A 2021 Blood-brain barrier opening with focused ultrasound in Parkinson's disease dementia *Nat Commun* **12** 779

Geoghegan R, Ter Haar G, Nightingale K, Marks L and Natarajan S 2022 Methods of monitoring thermal ablation of soft tissue tumors - A comprehensive review *Med Phys* **49** 769–91

Gerstenmayer M, Fellah B, Magnin R, Selingue E and Larrat B 2018 Acoustic Transmission Factor through the Rat Skull as a Function of Body Mass, Frequency and Position *Ultrasound in Medicine & Biology* **44** 2336–44

Gourevich D, Volovick A, Dogadkin O, Wang L, Mulvana H, Medan Y, Melzer A and Cochran S 2015 In Vitro Investigation of the Individual Contributions of Ultrasound-Induced Stable and Inertial Cavitation in Targeted Drug Delivery *Ultrasound in Medicine & Biology* **41** 1853–64

Goyal A, Yu F T H, Tenwalde M G, Chen X, Althouse A, Villanueva F S and Pacella J J 2017 Inertial Cavitation Ultrasound with Microbubbles Improves Reperfusion Efficacy When Combined with Tissue Plasminogen Activator in an In Vitro Model of Microvascular Obstruction *Ultrasound in Medicine & Biology* **43** 1391–400

Haworth K J, Raymond J L, Radhakrishnan K, Moody M R, Huang S-L, Peng T, Shekhar H, Klegerman M E, Kim H, McPherson D D and Holland C K 2016 Trans-Stent B-Mode Ultrasound and Passive Cavitation Imaging *Ultrasound Med Biol* **42** 518–27

Hockham N, Coussios C C and Arora M 2010 A real-time controller for sustaining thermally relevant acoustic cavitation during ultrasound therapy *IEEE transactions on ultrasonics, ferroelectrics, and frequency control* **57** 2685–94

Hoogenboom M, Eikelenboom D, den Brok M H, Heerschap A, Fütterer J J and Adema G J 2015 Mechanical high-intensity focused ultrasound destruction of soft tissue: working mechanisms and physiologic effects *Ultrasound Med Biol* **41** 1500–17

Huang Y, Alkins R, Schwartz M L and Hynynen K 2017 Opening the Blood-Brain Barrier with MR Imaging-guided Focused Ultrasound: Preclinical Testing on a Trans-Human Skull Porcine Model *Radiology* **282** 123–30

Huang Y, Meng Y, Pople C B, Bethune A, Jones R M, Abrahao A, Hamani C, Kalia S K, Kalia L V, Lipsman N and Hynynen K 2022 Cavitation Feedback Control of Focused Ultrasound Blood-Brain Barrier Opening for Drug Delivery in Patients with Parkinson's Disease *Pharmaceutics* **14** 2607

Hynynen K, McDannold N, Vykhodtseva N and Jolesz F A 2001 Noninvasive MR imaging-guided focal opening of the blood-brain barrier in rabbits *Radiology* **220** 640–6

Ilovitsh T, Ilovitsh A, Foiret J, Caskey C F, Kusunose J, Fite B Z, Zhang H, Mahakian L M, Tam S, Butts-Pauly K, Qin S and Ferrara K W 2018 Enhanced microbubble contrast agent oscillation following 250 kHz insonation *Sci Rep* **8** 16347

Izadifar Z, Izadifar Z, Chapman D and Babyn P 2020 An Introduction to High Intensity Focused Ultrasound: Systematic Review on Principles, Devices, and Clinical Applications *J Clin Med* **9** E460

Jangjou A, Meisami A H, Jamali K, Niakan M H, Abbasi M, Shafiee M, Salehi M, Hosseinzadeh A, Amani A M and Vaez A 2021 The promising shadow of

microbubble over medical sciences: from fighting wide scope of prevalence disease to cancer eradication *J Biomed Sci* **28** 49

Ji R, Karakatsani M E, Burgess M, Smith M, Murillo M F and Konofagou E E 2021 Cavitation-modulated inflammatory response following focused ultrasound blood-brain barrier opening *Journal of Controlled Release* **337** 458–71

Johnston K, Tapia-Siles C, Gerold B, Postema M, Cochran S, Cuschieri A and Prentice P 2014 Periodic shock-emission from acoustically driven cavitation clouds: A source of the subharmonic signal *Ultrasonics* **54** 2151–8

Jones R M, Deng L, Leung K, McMahon D, O'Reilly M A and Hynynen K 2018 Three-dimensional transcranial microbubble imaging for guiding volumetric ultrasound-mediated blood-brain barrier opening *Theranostics* **8** 2909–26

Jones R M, McMahon D and Hynynen K 2020 Ultrafast three-dimensional microbubble imaging in vivo predicts tissue damage volume distributions during nonthermal brain ablation *Theranostics* **10** 7211–30

Kamimura H A, Flament J, Valette J, Cafarelli A, Aron Badin R, Hantraye P and Larrat B 2019 Feedback control of microbubble cavitation for ultrasound-mediated blood-brain barrier disruption in non-human primates under magnetic resonance guidance *Journal of Cerebral Blood Flow and Metabolism: Official Journal of the International Society of Cerebral Blood Flow and Metabolism* **39** 1191–203

Kamimura H A S, Wu S-Y, Grondin J, Ji R, Aurup C, Zheng W, Heidmann M, Pouliopoulos A N and Konofagou E 2020 Real-time passive acoustic mapping using sparse matrix multiplication *IEEE transactions on ultrasonics, ferroelectrics, and frequency control* **PP**

Kamimura H A S, Wu S-Y, Grondin J, Ji R, Aurup C, Zheng W, Heidmann M, Pouliopoulos A N and Konofagou E E 2021 Real-Time Passive Acoustic Mapping Using Sparse Matrix Multiplication *IEEE Trans Ultrason Ferroelectr Freq Control* **68** 164–77

Klaseboer E and Khoo B 2004 An oscillating bubble near an elastic material *Journal of Applied Physics* **96** 5808–18

Lauterborn W and Cramer E 1981 Subharmonic Route to Chaos Observed in Acoustics *Phys. Rev. Lett.* **47** 1445–8

Lauterborn W and Kurz T 2010 Physics of bubble oscillations *Rep. Prog. Phys.* **73** 106501

Lee H, Guo Y, Ross J L, Schoen S, Degertekin F L and Arvanitis C 2022 Spatially targeted brain cancer immunotherapy with closed-loop controlled focused ultrasound and immune checkpoint blockade *Sci Adv* **8** eadd2288

Lee P, Wei H, Pouliopoulos A N, Forsyth B T, Yang Y, Zhang C, Laine A F, Konofagou E E, Wu C and Guo J 2023 Deep Learning Enables Reduced Gadolinium Dose for Contrast-Enhanced Blood-Brain Barrier Opening *ArXiv* arXiv:2301.07248v1

Leighton T 1994 The Acoustic Bubble *Journal of The Acoustical Society of America - J ACOUST SOC AMER* vol 96

Lin H-C, Fan C-H, Ho Y-J and Yeh C-K 2020 Dual-Frequency Chirp Excitation for Passive Cavitation Imaging in the Brain *IEEE transactions on ultrasonics, ferroelectrics, and frequency control* **67** 1127–40

Lin Y, Lin L, Cheng M, Jin L, Du L, Han T, Xu L, Yu A C H and Qin P 2017 Effect of acoustic parameters on the cavitation behavior of SonoVue microbubbles induced by pulsed ultrasound *Ultrasonics Sonochemistry* **35** 176–84

Lipsman N, Meng Y, Bethune A J, Huang Y, Lam B, Masellis M, Herrmann N, Heyn C, Aubert I, Boutet A, Smith G S, Hynynen K and Black S E 2018 Blood-brain barrier opening in Alzheimer's disease using MR-guided focused ultrasound *Nat Commun* **9** 2336

Liu H-L, Jan C-K, Chu P-C, Hong J-C, Lee P-Y, Hsu J-D, Lin C-C, Huang C-Y, Chen P-Y and Wei K-C 2014 Design and Experimental Evaluation of a 256-Channel Dual-Frequency Ultrasound Phased-Array System for Transcranial Blood–Brain Barrier Opening and Brain Drug Delivery *IEEE Transactions on Biomedical Engineering* **61** 1350–60

Liu Y, Fite B Z, Mahakian L M, Johnson S M, Larrat B, Dumont E and Ferrara K W 2015 Concurrent Visualization of Acoustic Radiation Force Displacement and Shear Wave Propagation with 7T MRI *PLoS One* **10** e0139667

Lo A H, Kripfgans O D, Carson P L and Fowlkes J B 2006 Spatial control of gas bubbles and their effects on acoustic fields *Ultrasound Med Biol* **32** 95–106

Lynch M, Heinen S, Markham-Coultes K, O'Reilly M, Van Slyke P, Dumont D J, Hynynen K and Aubert I 2021 Vasculotide restores the blood-brain barrier after focused ultrasound-induced permeability in a mouse model of Alzheimer's disease *Int. J. Med. Sci.* **18** 482–93

Maciulevicius M, Tamosiunas M, Jurkonis R, Venslauskas M S and Satkauskas S 2015 Analysis of Metrics for Molecular Sonotransfer in Vitro *Molecular Pharmaceutics* **12** 3620–7

Mainprize T, Lipsman N, Huang Y, Meng Y, Bethune A, Ironside S, Heyn C, Alkins R, Trudeau M, Sahgal A, Perry J and Hynynen K 2019a Blood-Brain Barrier Opening in Primary Brain Tumors with Non-invasive MR-Guided Focused Ultrasound: A Clinical Safety and Feasibility Study *Sci Rep* **9** 321

Mainprize T, Lipsman N, Huang Y, Meng Y, Bethune A, Ironside S, Heyn C, Alkins R, Trudeau M, Sahgal A, Perry J and Hynynen K 2019b Blood-Brain Barrier Opening in Primary Brain Tumors with Non-invasive MR-Guided Focused Ultrasound: A Clinical Safety and Feasibility Study *Sci Rep* **9** 321

Marquet F, Teichert T, Wu S-Y, Tung Y-S, Downs M, Wang S, Chen C, Ferrera V and Konofagou E E 2014 Real-time, transcranial monitoring of safe blood-brain barrier opening in non-human primates *PloS One* **9** e84310

McDannold N, Vykhodtseva N and Hynynen K 2008 Blood-Brain Barrier Disruption Induced by Focused Ultrasound and Circulating Preformed Microbubbles Appears to Be Characterized by the Mechanical Index *Ultrasound in Medicine & Biology* **34** 834–40

McDannold N, Vykhodtseva N and Hynynen K 2006 Targeted disruption of the blood-brain barrier with focused ultrasound: association with cavitation activity *Physics in Medicine and Biology* **51** 793–807

McDannold N, Zhang Y, Supko J G, Power C, Sun T, Vykhodtseva N, Golby A J and Reardon D A 2020 Blood-brain barrier disruption and delivery of irinotecan in a rat model using a clinical transcranial MRI-guided focused ultrasound system *Sci Rep* **10** 8766

McMahon D, Lassus A, Gaud E, Jeannot V and Hynynen K 2020 Microbubble formulation influences inflammatory response to focused ultrasound exposure in the brain *Sci Rep* **10** 21534

Miller D L and Thomas R M 1995 Ultrasound contrast agents nucleate inertial cavitation in vitro *Ultrasound in Medicine and Biology* **21** 1059–65

Novell A, Kamimura H a. S, Cafarelli A, Gerstenmayer M, Flament J, Valette J, Agou P, Conti A, Selingue E, Aron Badin R, Hantraye P and Larrat B 2020 A new safety index based on intrapulse monitoring of ultra-harmonic cavitation during ultrasound-induced blood-brain barrier opening procedures *Scientific Reports* **10** 10088

O'Reilly M A and Hynynen K 2010 A PVDF receiver for ultrasound monitoring of transcranial focused ultrasound therapy *IEEE transactions on bio-medical engineering* **57** 2286–94

O'Reilly M A and Hynynen K 2012 Blood-brain barrier: real-time feedback-controlled focused ultrasound disruption by using an acoustic emissions-based controller *Radiology* **263** 96–106

O'Reilly M A, Jones R M and Hynynen K 2014 Three-dimensional transcranial ultrasound imaging of microbubble clouds using a sparse hemispherical array *IEEE transactions on bio-medical engineering* **61** 1285–94

O'Reilly M A, Muller A and Hynynen K 2011 Ultrasound insertion loss of rat parietal bone appears to be proportional to animal mass at submegahertz frequencies *Ultrasound Med Biol* **37** 1930–7

Pahk K J, Gélat P, Kim H and Saffari N 2018 Bubble dynamics in boiling histotripsy *Ultrasound in Medicine & Biology* **44** 2673–96

Pandit R, Chen L and Götz J 2020 The blood-brain barrier: Physiology and strategies for drug delivery *Adv Drug Deliv Rev* **165–166** 1–14

Parlitz U, Englisch V, Scheffczyk C and Lauterborn W 1990 Bifurcation structure of bubble oscillators *The Journal of the Acoustical Society of America* **88** 1061–77

Pascal A, Li N, Lechtenberg K J, Rosenberg J, Airan R D, James M L, Bouley D M and Pauly K B 2020 Histologic evaluation of activation of acute inflammatory response in a mouse model following ultrasound-mediated blood-brain barrier using different acoustic pressures and microbubble doses *Nanotheranostics* **4** 210–23

Patel A, Schoen S J and Arvanitis C D 2018 Closed Loop Spatial and Temporal Control of Cavitation Activity with Passive Acoustic Mapping *IEEE Trans Biomed Eng*

Pavlos Anastasiadis, Dheeraj Gandhi, Yutong Guo, Abdul-Kareem Ahmed, Soren M Bentzen, Costas Arvanitis, and Graeme F Woodworth 2021 Localized blood-brain barrier opening in infiltrating gliomas with MRI-guided acoustic emissions-controlled focused ultrasound - PubMed *PNAS* **118** Online: https://pubmed.ncbi.nlm.nih.gov/34504017/

Pichardo S, Sin V W and Hynynen K 2010 Multi-frequency characterization of the speed of sound and attenuation coefficient for longitudinal transmission of freshly excised human skulls *Phys. Med. Biol.* **56** 219–50

Pinton G, Aubry J-F, Bossy E, Muller M, Pernot M and Tanter M 2012 Attenuation, scattering, and absorption of ultrasound in the skull bone *Med Phys* **39** 299–307

Poliachik S L, Chandler W L, Mourad P D, Bailey M R, Bloch S, Cleveland R O, Kaczkowski P, Keilman G, Porter T and Crum L A 1999 Effect of high-intensity focused ultrasound on whole blood with and without microbubble contrast agent *Ultrasound in Medicine & Biology* **25** 991–8

Porto A, Shirai L T, de Oliveira F B and Marroig G 2013 Size variation, growth strategies, and the evolution of modularity in the mammalian skull *Evolution* **67** 3305–22

Postema M, Marmottant P, Lancée C T, Hilgenfeldt S and Jong N de 2004 Ultrasound-induced microbubble coalescence *Ultrasound in Medicine & Biology* **30** 1337–44

Pouliopoulos A N, Burgess M T and Konofagou E E 2018 Pulse inversion enhances the passive mapping of microbubble-based ultrasound therapy *Applied Physics Letters* **113** 044102

Pouliopoulos A N, Jimenez D A, Frank A, Robertson A, Zhang L, Kline-Schoder A R, Bhaskar V, Harpale M, Caso E, Papapanou N, Anderson R, Li R and Konofagou E E 2020a Temporal stability of lipid-shelled microbubbles during acoustically-mediated blood-brain barrier opening *Frontiers in Physics* **8**

Pouliopoulos A N, Li C, Tinguely M, Garbin V, Tang M-X and Choi J J 2016 Rapid short-pulse sequences enhance the spatiotemporal uniformity of acoustically driven microbubble activity during flow conditions *The Journal of the Acoustical Society of America* **140** 2469

Pouliopoulos A N, Wu S-Y, Burgess M T, Karakatsani M E, Kamimura H A S and Konofagou E E 2020b A Clinical System for Non-invasive Blood-Brain Barrier Opening Using a Neuronavigation-Guided Single-Element Focused Ultrasound Transducer *Ultrasound in Medicine & Biology* **46** 73–89

Prokop A F, Soltani A and Roy R A 2007 Cavitational mechanisms in ultrasound-accelerated fibrinolysis *Ultrasound in Medicine & Biology* **33** 924–33

Qiu Y, Luo Y, Zhang Y, Cui W, Zhang D, Wu J, Zhang J and Tu J 2010 The correlation between acoustic cavitation and sonoporation involved in ultrasound-mediated DNA

transfection with polyethylenimine (PEI) in vitro *Journal of Controlled Release: Official Journal of the Controlled Release Society* **145** 40–8

Quadri S A, Waqas M, Khan I, Khan M A, Suriya S S, Farooqui M and Fiani B 2018 High-intensity focused ultrasound: past, present, and future in neurosurgery *Neurosurg Focus* **44** E16

Rabkin B A, Zderic V and Vaezy S 2005 Hyperecho in ultrasound images of HIFU therapy: involvement of cavitation *Ultrasound in Medicine & Biology* **31** 947–56

Rademaker G, Jenne J W, Rastert R, Röder D and Schad L 2003 [Comparison of noninvasive MRT procedures for temperature measuremnt for the application of medical heat therapies] *Z Med Phys* **13** 183–7

Rieke V and Butts Pauly K 2008 MR thermometry *J Magn Reson Imaging* **27** 376–90

Sheikov N, McDannold N, Vykhodtseva N, Jolesz F and Hynynen K 2004 Cellular mechanisms of the blood-brain barrier opening induced by ultrasound in presence of microbubbles *Ultrasound Med Biol* **30** 979–89

Shi W T and Forsberg F 2000 Ultrasonic characterization of the nonlinear properties of contrast microbubbles *Ultrasound Med Biol* **26** 93–104

Sierra C, Acosta C, Chen C, Wu S-Y, Karakatsani M E, Bernal M and Konofagou E E 2017 Lipid microbubbles as a vehicle for targeted drug delivery using focused ultrasound-induced blood-brain barrier opening *Journal of Cerebral Blood Flow and Metabolism: Official Journal of the International Society of Cerebral Blood Flow and Metabolism* **37** 1236–50

Soltani A, Volz K R and Hansmann D R 2008 Effect of modulated ultrasound parameters on ultrasound-induced thrombolysis *Phys Med Biol* **53** 6837–47

Sun T, Samiotaki G, Wang S, Acosta C, Chen C C and Konofagou E E 2015 Acoustic cavitation-based monitoring of the reversibility and permeability of ultrasound-induced blood-brain barrier opening *Physics in Medicine and Biology* **60** 9079–94

Sun T, Zhang Y, Power C, Alexander P M, Sutton J T, Aryal M, Vykhodtseva N, Miller E L and McDannold N J 2017 Closed-loop control of targeted ultrasound drug delivery across the blood-brain/tumor barriers in a rat glioma model *Proceedings of the National Academy of Sciences of the United States of America* **114** E10281–90

Sutton J T, Raymond J L, Verleye M C, Pyne-Geithman G J and Holland C K 2014 Pulsed ultrasound enhances the delivery of nitric oxide from bubble liposomes to ex vivo porcine carotid tissue *International Journal of Nanomedicine* **9** 4671–83

Top C B, White P J and McDannold N J 2016 Nonthermal ablation of deep brain targets: A simulation study on a large animal model *Medical Physics* **43** 870–82

Tran B C, Seo J, Hall T L, Fowlkes J B and Cain C A 2003 Microbubble-enhanced cavitation for noninvasive ultrasound surgery *IEEE transactions on ultrasonics, ferroelectrics, and frequency control* **50** 1296–304

Tsai C-H, Zhang J-W, Liao Y-Y and Liu H-L 2016 Real-time monitoring of focused ultrasound blood-brain barrier opening via subharmonic acoustic emission detection: implementation of confocal dual-frequency piezoelectric transducers *Physics in Medicine and Biology* **61** 2926–46

Tu J, Hwang J H, Matula T J, Brayman A A and Crum L A 2006 Intravascular inertial cavitation activity detection and quantification in vivo with Optison *Ultrasound in Medicine & Biology* **32** 1601–9

Tung Y-S, Choi J J, Baseri B and Konofagou E E 2010 Identifying the inertial cavitation threshold and skull effects in a vessel phantom using focused ultrasound and microbubbles *Ultrasound Med Biol* **36** 840–52

Tung Y-S, Liu H-L, Wu C-C, Ju K-C, Chen W-S and Lin W-L 2006 Contrast-agent-enhanced ultrasound thermal ablation *Ultrasound Med Biol* **32** 1103–10

Tung Y-S, Marquet F, Teichert T, Ferrera V and Konofagou E E 2011 Feasibility of noninvasive cavitation-guided blood-brain barrier opening using focused ultrasound and microbubbles in nonhuman primates *Applied Physics Letters* **98** 163704

Vignon F, Shi W T, Powers J E, Everbach E C, Liu J, Gao S, Xie F and Porter T R 2013 Microbubble cavitation imaging *IEEE Trans Ultrason Ferroelectr Freq Control* **60** 661–70

van Wamel A, Kooiman K, Harteveld M, Emmer M, ten Cate F J, Versluis M and de Jong N 2006 Vibrating microbubbles poking individual cells: Drug transfer into cells via sonoporation *Journal of Controlled Release* **112** 149–55

Wang W, Jing T, Xia X, Tang L, Huang Z, Liu F, Wang Z, Ran H, Li M and Xia J 2019 Melanin-loaded biocompatible photosensitive nanoparticles for controlled drug release in combined photothermal-chemotherapy guided by photoacoustic/ultrasound dual-modality imaging *Biomaterials Science* **7** 4060–74

White P J, Clement G T and Hynynen K 2006 Longitudinal and shear mode ultrasound propagation in human skull bone *Ultrasound in Medicine & Biology* **32** 1085–96

Wu S-K, Chu P-C, Chai W-Y, Kang S-T, Tsai C-H, Fan C-H, Yeh C-K and Liu H-L 2017 Characterization of Different Microbubbles in Assisting Focused Ultrasound-Induced Blood-Brain Barrier Opening *Scientific Reports* **7** 46689

Wu S-Y, Aurup C, Sanchez C S, Grondin J, Zheng W, Kamimura H, Ferrera V P and Konofagou E E 2018a Efficient Blood-Brain Barrier Opening in Primates with Neuronavigation-Guided Ultrasound and Real-Time Acoustic Mapping *Sci Rep* **8** 7978

Wu S-Y, Fix S M, Arena C B, Chen C C, Zheng W, Olumolade O O, Papadopoulou V, Novell A, Dayton P A and Konofagou E E 2018b Focused ultrasound-facilitated brain drug delivery using optimized nanodroplets: vaporization efficiency dictates large molecular delivery *Physics in Medicine and Biology* **63** 035002

Wu S-Y, Sanchez C S, Samiotaki G, Buch A, Ferrera V P and Konofagou E E 2016 Characterizing Focused-Ultrasound Mediated Drug Delivery to the Heterogeneous Primate Brain In Vivo with Acoustic Monitoring *Scientific Reports* **6** 37094

Wu S-Y, Tung Y-S, Marquet F, Downs M, Sanchez C, Chen C, Ferrera V and Konofagou E 2014 Transcranial cavitation detection in primates during blood-brain barrier opening--a performance assessment study *IEEE transactions on ultrasonics, ferroelectrics, and frequency control* **61** 966–78

Xu H, He L, Zhong B, Qiu J and Tu J 2019a Classification and prediction of inertial cavitation activity induced by pulsed high-intensity focused ultrasound *Ultrasonics Sonochemistry* **56** 77–83

Xu S, Ye D, Wan L, Shentu Y, Yue Y, Wan M and Chen H 2019b Correlation Between Brain Tissue Damage and Inertial Cavitation Dose Quantified Using Passive Cavitation Imaging *Ultrasound in Medicine & Biology* **45** 2758–66

Yang Y, Li Q, Guo X, Tu J and Zhang D 2020 Mechanisms underlying sonoporation: Interaction between microbubbles and cells *Ultrason Sonochem* **67** 105096

Yang Y, Zhang X, Ye D, Laforest R, Williamson J, Liu Y and Chen H 2019 Cavitation dose painting for focused ultrasound-induced blood-brain barrier disruption *Scientific Reports* **9** 2840

Yasui K 2023 Origin of the broad-band noise in acoustic cavitation *Ultrasonics Sonochemistry* **93** 106276

Zhang Q Q, Djuth F T, Zhou Q F, Hu C H, Cha J H and Shung K K 2006 High frequency broadband PZT thick film ultrasonic transducers for medical imaging applications *Ultrasonics* **44 Suppl 1** e711-715

Zhang S, Cui Z, Xu T, Liu P, Li D, Shang S, Xu R, Zong Y, Niu G, Wang S, He X and Wan M 2017 Inverse effects of flowing phase-shift nanodroplets and lipid-shelled microbubbles on subsequent cavitation during focused ultrasound exposures *Ultrasonics Sonochemistry* **34** 400–9